UC Davis

UC Davis Previously Published Works

Title

Carbon—water coupling in California almond orchards: a multi-scale assessment of ecosystem water use efficiency using eddy covariance and remote sensing

Permalink

https://escholarship.org/uc/item/6mh3z1sp

Journal

The Science of The Total Environment, 990

ISSN

0048-9697

Authors

Peddinti, Srinivasa Rao

Kisekka, Isaya

Publication Date

2025-08-01

DOI

10.1016/j.scitotenv.2025.179914

Copyright Information

This work is made available under the terms of a Creative Commons Attribution License, available at https://creativecommons.org/licenses/by/4.0/

Peer reviewed

eScholarship.org Powered by the California Digital Library
University of California

Science of the Total Environment 990 (2025) 179914

Contents lists available at ScienceDirect

Science of the Total Environment

journal homepage: www.elsevier.com/locate/scitotenv

Carbon–water coupling in California almond orchards: a multi-scale assessment of ecosystem water use efficiency using eddy covariance and remote sensing

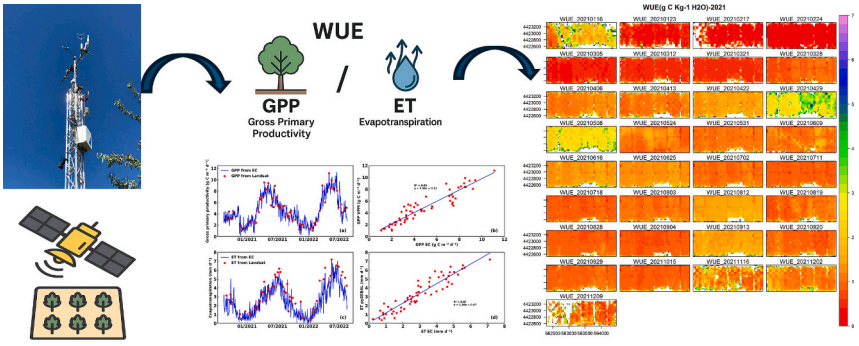
Srinivasa Rao Peddinti [a], Isaya Kisekka [a,b,*]

[a] Department of Land, Air & Water Resources, University of California Davis, Davis, CA 95616, USA
[b] Department of Biological and Agricultural Engineering, University of California Davis, Davis, CA 95616, USA

HIGHLIGHTS

- Water use efficiency varies with almond phenology and is lowest during kernel fill.
- Seasonal WUE varies from 0.5 to 5.9 g C $kg^{-1}H_2O$, peaking during dormancy.
- Spatial WUE maps reveal heterogeneity, informing precision irrigation.
- Temperature and VPD are dominant controls on WUE.

GRAPHICAL ABSTRACT



ARTICLE INFO

Editor: Elena Paoletti

Keywords:
Gross primary productivity
Evapotranspiration
pySEBAL
Crop water use
Precision agriculture
Water management

ABSTRACT

Water use efficiency (WUE) at the ecosystem level is a critical ecophysiological indicator that integrates carbon-water coupling processes and provides essential insights for sustainable agriculture in water-limited environments. This study investigated the dynamics of WUE in California almond orchards, a high-value and water-intensive crop system of global economic significance, by combining eddy covariance (EC) measurements with satellite remote sensing to analyze seasonal and interannual patterns from 2020 to 2022. Gross primary productivity (GPP) was estimated using the Vegetation Photosynthesis Model (VPM), while evapotranspiration (ET) was derived using the pySEBAL surface energy balance model applied to Landsat imagery. The ratio of these fluxes provided spatially distributed WUE estimates. Daily GPP ranged from ~0.5 to 11.5 g C m^{-2} d^{-1}, while ET ranged from ~0.5 to 7.5 mm d^{-1}, with both fluxes peaking during mid-summer. WUE values exhibited distinct seasonal patterns (ranging from ~0.5 to 5.9 g C kg^{-1} H_2O), with higher efficiency during dormancy and lower values during fruit development stages, averaging 2.14 g C kg^{-1} H_2O over the study period. GPP and ET showed similar seasonal patterns and responded in tandem to key climatic variables (solar radiation, air temperature, and humidity), suggesting common environmental drivers govern these processes. WUE exhibited more complex behavior: it increased slightly with greater precipitation and humidity and declined under high solar radiation,

* Corresponding author at: Department of Land Air & Water Resources, Department of Biological and Agricultural Engineering University of California Davis, One Shields Avenue, Davis, CA 95616-5270, USA.
E-mail address: ikisekka@ucdavis.edu (I. Kisekka).

https://doi.org/10.1016/j.scitotenv.2025.179914
Received 19 April 2025; Received in revised form 10 June 2025; Accepted 12 June 2025
Available online 18 June 2025
0048-9697/© 2025 The Authors. Published by Elsevier B.V. This is an open access article under the CC BY license (http://creativecommons.org/licenses/by/4.0/).

high vapor pressure deficit (VPD), and extreme temperatures. The remote sensing-derived GPP and ET agreed well with EC tower measurements ($R^2 \approx 0.87$–0.88), affirming the reliability of the integrated approach. This study advances our understanding of carbon-water coupling in perennial almond orchard systems. It provides valuable ecological indicators for precision irrigation management in the face of increasing water scarcity and climate variability.

1. Introduction

Water scarcity represents one of the most pressing challenges for global agriculture in the 21st century, particularly as climate change intensifies hydrological extremes and population growth increases food demand (Evans and Sadler, 2008). In this context, water use efficiency (WUE), the ratio of biomass produced to water consumed, has emerged as a critical ecophysiological indicator that integrates carbon and water cycles while providing essential insights for sustainable agricultural management. Understanding WUE dynamics is especially crucial for high-value, water-intensive perennial crops like almonds (Almond board, 2018; Doll, 2017; Vuppalapati, 2023), which face unique sustainability challenges compared to annual crops or natural ecosystems. Almond orchards constitute a distinct agroecosystem compared to annual and other perennial crops, due to their specific physiological traits, phenological cycles, and intensive management practices (Sánchez-Navarro et al., 2022; Vanella et al., 2022). Unlike annual crops, almonds possess extensive woody biomass and deep root systems, characteristic of perennials, yet their complete winter dormancy and early spring flowering under potential water stress distinguish them from evergreen or semi-deciduous perennials like citrus or olive (Esparza et al., 2001). These traits result in pronounced seasonal carbon-water decoupling, with a compressed phenological window for nut development and harvest. Furthermore, almond orchards are managed at high planting density with precise fertigation and pruning regimes tailored to maximize kernel yield within this short phenological timeframe (Álvarez et al., 2020), contrasting with the less phenologically constrained management of annual crops and the differing physiological demands of evergreen perennial crops. Consequently, almond orchards display pronounced periods of elevated water demand and a distinct seasonal pattern in WUE. These physiological and management-driven traits necessitate specialized, phenology-informed approaches to accurately quantify and interpret WUE dynamics in almond agroecosystems.

The economic and environmental significance of almond production further underscores the importance of studying WUE in these systems. California produces approximately 80 % of the world's almonds, with over 1.52 million acres (615,122 ha) dedicated to almond cultivation as of 2024 (Niederholzer et al., 2024; Urbana-Champaign, 2025). This extensive production represents a critical agricultural sector worth over $5 billion annually (Klein, 2024). But it also faces mounting sustainability challenges. Almond orchards require substantial irrigation water throughout their long growing season, with water costs representing up to 25 % of production expenses (Goodrich, 2020). As California continues to experience severe drought conditions and increasing water regulations, optimizing WUE in almond production has become essential not only for environmental sustainability but also for the economic viability of the industry (AgNet West, 2024). Accurately measuring ecosystem-scale carbon uptake (gross primary productivity, GPP) and water use (evapotranspiration, ET) in almond orchards poses distinct challenges, differing from the greater complexity of multi-species forest ecosystems. The eddy covariance (EC) technique provides direct, high-frequency measurements of CO_2 and H_2O fluxes but is limited to the tower footprint. Satellite remote sensing offers complementary capabilities for estimating these fluxes across broader spatial scales. Light-use efficiency models (He et al., 2013; Turner et al., 2003) can derive GPP from optical vegetation indices, while energy balance models (Allen et al., 2007; Bastiaanssen et al., 1998a, 1998b; Norman et al., 1995; Su, 2002) estimate ET from thermal infrared data. The integration of these approaches, combining ground-based EC measurements with satellite-derived spatial estimates, creates a powerful framework for analyzing WUE across multiple scales.

This integrated approach, combining high-frequency EC measurements with satellite-derived estimates of GPP and ET, has proven effective in examining WUE across diverse ecosystems and agricultural settings. For instance, Mei et al. (2023) investigated the spatiotemporal variability and drivers of WUE in Inner Mongolia, while Elfarkh et al. (2023) successfully applied this methodology to high-density olive orchards. Similarly, Abraha et al. (2016) utilized this integrated framework to compare WUE dynamics between annual corn and perennial grassland systems, and Peddinti et al. (2020) focused on citrus orchards. Tong et al. (2009) examined WUE patterns specifically within maize cropping systems. Furthermore, Liu et al. (2017) and Song et al. (2017) extended the application of this methodology to old-growth forests and subtropical evergreen forests, respectively.

Across these various ecosystems, key drivers of WUE, such as soil moisture, vegetation structure, and drought-related stressors, have been identified. For example, Huang et al. (2017) analyzed global-scale relationships between ecosystem WUE and drought conditions, whereas Liu et al. (2020) employed process-based carbon cycle models to study global trends in WUE. In agricultural contexts, comparative analyses of WUE across maize, perennial crops, and restored prairie ecosystems have been conducted by Abraha et al. (2016), Hamilton et al. (2015), and Hoover et al. (2023). Similarly, Tong et al. (2009) evaluated WUE within irrigated wheat-maize rotation systems. More recently, Kandhway et al. (2025) modeled the impacts of climate change and elevated atmospheric CO_2 on water use and phenological dynamics specifically in almond and pistachio orchards, highlighting the intricate interactions between evapotranspiration, phenology, and carbon-water exchanges.

However, despite these advancements, comprehensive studies integrating EC measurements with satellite-derived GPP and ET specifically for perennial or woody orchard systems such as almonds remain scarce. To our knowledge, this is the first study that integrates eddy covariance measurements with satellite-derived estimates of GPP (from VPM) and ET (from pySEBAL) to comprehensively evaluate ecosystem-scale water use efficiency (WUE) in almond orchards. Furthermore, by emphasizing the mapping of spatial heterogeneity in orchard WUE, this research offers a novel methodological contribution to enhance precision irrigation management practices in perennial systems, an issue that has received limited attention in previous research.

The mechanistic drivers of WUE operate differently across ecosystem types due to variations in physiological responses and environmental interactions. In natural forest ecosystems, WUE is strongly influenced by stomatal regulation in response to vapor pressure deficit (VPD), with many species showing decreased WUE under high VPD conditions as stomatal closure limits carbon uptake more than water loss (Liu et al., 2017). Annual crops typically exhibit different patterns, with WUE often peaking during specific developmental stages and showing strong responses to management practices like irrigation timing (Tong et al., 2009). Perennial orchard systems like almonds likely have distinct WUE response patterns due to their unique combination of woody biomass, seasonal phenology, and intensive management, but these mechanisms remain poorly characterized. Several key knowledge gaps exist regarding WUE in almond orchards. First, the seasonal dynamics of WUE in relation to the distinct phenological stages of almonds (dormancy, flowering, fruit development, post-harvest) have not been comprehensively analyzed. Second, the mechanistic responses of almond WUE to

environmental drivers like temperature, VPD, and solar radiation remain unclear, particularly how these responses might differ from other ecosystem types. Third, the spatial heterogeneity of WUE within orchard systems has received limited attention, despite its importance for precision irrigation management. Finally, the interannual variability of WUE in response to changing climate conditions represents a critical knowledge gap for long-term orchard sustainability.

To address critical knowledge gaps concerning WUE in almond orchards, this study employs an integrated methodological framework that combines high-frequency EC measurements with satellite remote sensing to examine seasonal and interannual WUE dynamics in California almond orchards from 2020 to 2022. Specifically, this research aims to: (1) characterize the seasonal patterns of ET, GPP, and WUE, linking these patterns explicitly to distinct almond phenological stages; (2) develop and validate spatially explicit WUE estimates by integrating GPP derived from the Vegetation Photosynthesis Model (VPM) with ET estimated through the pySEBAL model; (3) quantify mechanistic relationships between key environmental variables (temperature, vapor pressure deficit [VPD], solar radiation), soil water storage within the rootzone, and almond orchard WUE; and (4) analyze spatial and temporal variability in orchard WUE to support precision irrigation management.

Despite the recognized importance of WUE in agricultural systems, significant gaps persist regarding perennial orchard crops like almonds, whose carbon-water dynamics fundamentally differ from annual cropping systems and natural ecosystems. Notably, no previous studies have integrated EC flux measurements with spatially explicit remote sensing models (e.g., VPM and pySEBAL) to comprehensively assess WUE in almond orchards. To explicitly address these gaps, this study tests the following novel hypotheses:

(1) Almond orchards exhibit distinctive seasonal WUE dynamics that are closely tied to their specific phenological stages, differing significantly from those observed in annual cropping systems.

(2) The responses of almond orchard WUE to environmental drivers such as temperature, VPD, and solar radiation are uniquely shaped by their perennial woody biomass and intensive agricultural management practices.

(3) Spatial heterogeneity in WUE within almond orchards is substantial, driven primarily by variability in canopy structure, soil characteristics, and irrigation practices, thereby highlighting the necessity for targeted precision irrigation strategies.

(4) Almond orchard WUE displays notable interannual variability, emphasizing the critical importance of adaptive irrigation management strategies to effectively cope with ongoing climate variability.

This research contributes significantly to our understanding of carbon-water coupling in perennial orchard systems, providing novel ecological insights that can inform sustainable water management practices. By elucidating the unique WUE dynamics of almond orchards, this study offers critical guidance for enhancing irrigation strategies, ultimately aiding water conservation efforts while ensuring productivity in the context of increasing water scarcity and climatic pressures.

2. Material and methods

2.1. Study site description

This study was conducted in a commercial almond orchard managed by California Almond Packers and Exporters (CAPEX), an affiliate of Esteve Ranch, located near Corning in the northern Sacramento Valley of California, United States (39.93°N, −122.19°W, elevation 68 m) (Fig. 1). This region was selected as representative of California's major almond-growing areas, characterized by a Mediterranean climate with hot, dry summers and mild, wet winters. The site experiences a mean annual temperature of 16.6 °C and receives approximately 548 mm of annual precipitation, predominantly during winter months (November–March). Summer growing seasons feature abundant solar radiation, low humidity, and minimal rainfall, creating conditions that necessitate irrigation for optimal orchard productivity. The experimental orchard consists of 12-year-old almond trees planted in a systematic grid pattern with 6.7 m between rows and 3.4 m within rows (approximately 440 trees per hectare), representing the standard commercial density for mature almond production in California. The orchard design incorporates a strategic mix of complementary cultivars to enhance cross-pollination efficiency: 50 % Nonpareil (the industry standard and primary commercial variety), 25 % Monterey, and 25 % Butte (Tombesi et al., 2011). This cultivar distribution is typical of commercial almond production systems in California, designed to optimize yield while maintaining nut quality. The trees had reached full maturity with an average height of 6.5 m and canopy diameter of 5.8 m at the time of the study, representing the productive phase of commercial almond orchards.

The orchard soil profile consists of two predominant soil types: sandy clay loam (53.1 % sand, 27.6 % clay, 19.3 % silt) and clay loam (42.8 % sand, 26.9 % clay, 30.3 % silt) (Peddinti and Kisekka, 2022; Vanella et al., 2022), both classified as fine-loamy, mixed, thermic Typic Haploxeralfs according to USDA soil taxonomy (Soil Survey Staff, 1999). Soil pH ranges from 6.4 to 7.2, with organic matter content of 1.2–1.8 %. These soil characteristics are representative of many almond-growing regions in California's Central Valley. The orchard is irrigated using a micro-sprinkler system that delivers 45 l per hour per tree, with one

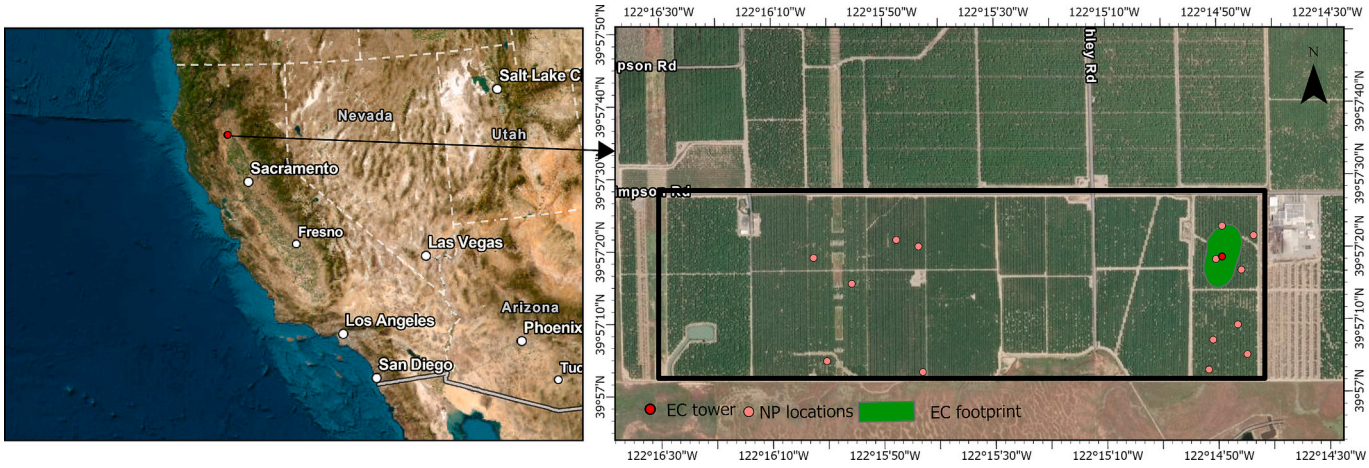


Fig. 1. Location of the study site and experimental setup. Map showing the location of the CAPEX almond orchard in the northern Sacramento Valley of California (left panel) and aerial view of the orchard with the location of the eddy covariance flux tower and neutron probe locations (right panel).

sprinkler positioned between every two trees. Irrigation was typically applied 2–3 times per week during peak summer months (June–August), with reduced frequency during spring and fall. Total irrigation applications ranged from approximately 900–1100 mm annually across the three-year study period, consistent with typical commercial practices for mature almond orchards in the region. Standard commercial management practices were maintained throughout the study period, including fertilization, pest management, and pruning. Annual nitrogen application averaged 280 kg N/ha, applied through fertigation in multiple applications from April through August (Muhammad et al., 2020). Winter pruning was conducted annually to maintain tree structure and optimize light penetration. These management practices ensured that the study site represented typical commercial production conditions, enhancing the applicability of our findings to the broader almond industry.

To monitor soil water content, neutron probe (NP) access tubes were installed at 14 locations across the orchard (Fig. 1). Weekly NP measurements were collected during the growing seasons from 2020 to 2022 at depths of 20, 45, and 76 cm. All probes were site-specifically calibrated to convert raw neutron count ratios into volumetric water content (VWC). The weekly VWC data were cleaned and then linearly interpolated to generate continuous daily time series. At each site, soil water storage (SWS, in cm) was calculated daily by multiplying VWC by the thickness of each measurement layer and summing across the three depths, covering the effective root zone to 76 cm. These site-level daily SWS values were then averaged across all 14 locations to derive orchard-scale SWS, which was used to assess temporal soil water availability and to evaluate correlations with water use efficiency (WUE) over the study period.

2.2. Eddy covariance measurements and data processing

A flux tower was erected within the CAPEX almond orchard to continuously measure carbon dioxide, water vapor, and energy fluxes across the soil-plant-atmosphere continuum (Fig. 1). The tower location was selected to maximize fetch in the predominant wind direction, ensuring that measured fluxes primarily represented the target almond orchard. The tower was positioned with a minimum fetch of 700 m in all directions within the uniform orchard block, exceeding the recommended fetch-to-height ratio of 100:1 for flux measurements over agricultural surfaces (Allen et al., 2011). The eddy covariance (EC) system consisted of a three-dimensional sonic anemometer (Gill R3–50, Gill Instruments Ltd., Hampshire, UK) paired with an open-path infrared gas analyzer (LI-7500, LI-COR Inc., Lincoln, NE, USA) mounted at 10 m above ground level, approximately 3 m above the average canopy height. This configuration allowed for measurements within the surface boundary layer while minimizing flow distortion effects from individual trees. The instruments were oriented toward the predominant wind direction (northwest) to reduce potential flow distortion from the tower structure.

The EC system measured three-dimensional wind velocity components and concentrations of CO2 and H2O at a frequency of 10 Hz, providing high-resolution data for flux calculations. Supporting meteorological measurements included air temperature and relative humidity (HMP155, Vaisala Inc., Helsinki, Finland), photosynthetically active radiation (LI-190R, LI-COR Inc.), net radiation using a four-component net radiometer (SN-500-SS, Apogee Instruments Inc., Logan, UT, USA), and precipitation (TR-525 M, Texas Electronics, Dallas, TX, USA). These instruments were mounted at various heights on the tower to capture the relevant environmental variables influencing carbon and water fluxes. Soil heat flux was measured using three soil heat flux plates (HFT-3, Radiation Energy Balance Systems, Bellevue, WA, USA) installed at 8 cm depth in representative locations (under canopy, at canopy edge, and in inter-row space) to account for spatial variability in soil heat flux. Each heat flux plate was paired with a soil temperature profile measured by thermocouples (TCAV-L, Campbell Scientific Inc., Logan, UT, USA) at 2.5 and 5 cm depths and soil moisture probes (GS-1, METER Group Inc., Pullman, WA, USA) at 5 cm depth to correct for heat storage in the soil layer above the plates. This comprehensive soil measurement approach ensured accurate quantification of the ground heat flux component of the energy balance.

Post-processing of EC data was conducted using EddyPro software (version 7.0.6, LI-COR Inc.) following standardized procedures for flux calculation and quality control. Raw 10 Hz data were processed to 30-min flux values with the following corrections applied: (1) coordinate rotation using the planar fit method to align the coordinate system with the mean wind streamlines; (2) time lag optimization between wind and scalar measurements; (3) spectral corrections for high and low-frequency losses following Moncrieff et al. (1997); and (4) density fluctuation corrections according to Webb et al. (1980) to account for heat and water vapor effects. The EC dataset had only 2 % missing values during the measurement period, which were gap-filled using the Marginal Distribution Sampling (MDS) method implemented in Tovi software (LI-COR Inc.). The energy balance closure, calculated as the ratio of turbulent energy fluxes (sensible heat + latent heat) to available energy (net radiation - soil heat flux), averaged 0.86 across the study period, with an R^2 value of 0.91 (Fig. 2). This closure ratio is within the typical range reported for EC measurements over agricultural systems and indicates satisfactory performance of the EC system (Mauder et al., 2024). Partitioning of net ecosystem exchange (NEE) into gross primary productivity (GPP) and ecosystem respiration (Reco) followed the approach of Reichstein et al. (2005), which uses nighttime flux data to establish a temperature response function for respiration and then applies this function to daytime periods. This partitioning approach was selected based on its robust performance in agricultural ecosystems and its implementation in standardized flux processing workflows. The resulting GPP estimates represent the total carbon uptake by the orchard ecosystem before accounting for respiratory losses.

2.3. Flux footprint analysis

A detailed footprint analysis was conducted to characterize the spatial source area contributing to the measured fluxes, ensuring appropriate comparison between tower-based measurements and satellite-derived estimates. The flux footprint represents the spatial distribution of surface sources and sinks that influence the scalar concentration measured at the tower, which varies with atmospheric stability, wind direction, and surface roughness. We employed the parameterized footprint model of Kljun et al. (2015), which provides a two-dimensional representation of the flux source area based on measurement height, roughness length, boundary layer height, and atmospheric stability parameters. This model was selected for its computational efficiency and validated performance across diverse ecosystems, including agricultural systems with heterogeneous vegetation structure. Footprint calculations were performed for each 30-min flux period using the measured friction velocity, standard deviation of lateral wind velocity, wind direction, and Obukhov length as inputs. The resulting footprints were aggregated to daily averages weighted by the magnitude of the carbon and water fluxes, providing a representative source area for each day of the study period. These daily footprints were then used to extract corresponding values from the satellite-derived GPP and ET maps for direct comparison with tower measurements. The average 80 % contribution footprint extended approximately 200–300 m upwind of the tower, with dimensions varying seasonally due to changes in atmospheric stability and canopy structure. During unstable daytime conditions typical of the growing season, the footprint was relatively compact (80 % contribution area of ~5–7 ha), while stable nighttime conditions resulted in more extended footprints. The predominant wind direction at the site was from the northwest, resulting in a primary footprint orientation along this axis.

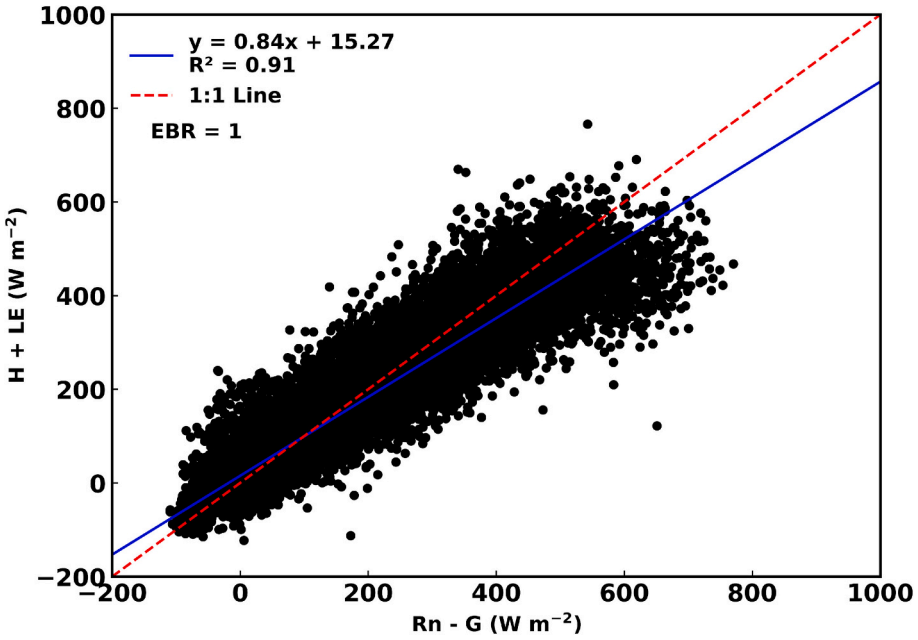


Fig. 2. Energy balance closure at the study site. Relationship between available energy (net radiation minus soil heat flux, Rn - G) and turbulent energy fluxes (sensible heat plus latent heat, H + LE) for 30-min periods during the three-year study period (2020–2022). The solid line represents the 1:1 relationship, and the dashed line represents the linear regression. Here the EBR is the energy balance ratio.

2.4. Remote sensing data acquisition and preprocessing

This study utilized data from the Landsat 8 Operational Land Imager (OLI) and Thermal Infrared Sensor (TIRS) to derive spatially explicit estimates of gross primary productivity (GPP) and evapotranspiration (ET) (Madugundu et al., 2017; Zhao and Running, 2010). Landsat 8 was selected as the primary data source due to its moderate spatial resolution (30 m for multispectral bands and 100 m for thermal bands, resampled to 30 m), suitable temporal resolution (7 or 16-day revisit cycle), and comprehensive spectral coverage, including visible, near-infrared, shortwave infrared, and thermal infrared bands. This spatial resolution is particularly well-suited for almond orchards, which typically have row spacing of 6–7 m, allowing for multiple pixels within individual orchard blocks and capturing the spatial heterogeneity of the orchard landscape.

Cloud-free Landsat 8 images covering the study area (path 44/45, row 32) were acquired from the United States Geological Survey (USGS) Earth Explorer platform (http://earthexplorer.usgs.gov) for the period from 2020 to 2022. Image selection followed a rigorous quality assessment protocol to ensure data integrity. First, only images with <10 % cloud cover over the study area were initially selected. Each image was then visually inspected to confirm the absence of clouds and cloud shadows over the orchard site. Second, images were screened using the Landsat Quality Assessment (QA) band to exclude pixels affected by detector failures, saturation, or other data quality issues. Third, images acquired during periods of high atmospheric aerosol loading (e.g., during wildfire smoke events) were excluded based on aerosol optical depth data from the MODIS aerosol product (MOD04). Lastly, priority was given to maintaining consistent temporal intervals between acquisitions, with emphasis on capturing key phenological stages of almond development, including dormancy, bloom, fruit development, harvest, and post-harvest periods.

Following this selection process, a total of 58 high-quality Landsat images were retained for analysis: 8 images for 2020, 33 for 2021, and 17 for 2022. The higher number of usable images in 2021 resulted from more favorable atmospheric conditions and the combined coverage provided by adjacent Landsat paths. The temporal distribution of the selected images offered comprehensive coverage of seasonal variations in orchard conditions across the three-year study period. All Landsat images were obtained as Collection 2, Level 2 surface reflectance products, which include radiometric calibration, geometric correction, and atmospheric correction using the Land Surface Reflectance Code (LaSRC) algorithm. These pre-processed products provide standardized surface reflectance values, minimizing the effects of atmospheric variability and enabling consistent multi-temporal analysis. Thermal bands were provided as surface temperature products derived using the Landsat 8 Single-Channel Algorithm, with atmospheric correction based on NCEP atmospheric profiles.

2.5. Evapotranspiration estimation with pySEBAL model

Based on the analysis of remote sensing of ET published papers, SEBAL stands out as one of the leading computational models for determining ET. Among its notable variations, the pySEBAL model, a Python-based version developed by the IHE-Delft Institute for Water Education, represents a significant advancement in the field and is readily available for scholarly use (https://github.com/wateraccounting/PySEBAL_dev). The SEBAL methodology is based on a fundamental concept of resolving the energy balance equation, as delineated in Eq. (1). Within this framework, the latent heat flux (LE), representing the energy utilized in the process of ET, is determined as the residual of the energy balance, Rn is net radiation, G is ground heat flux, and H is sensible heat flux in units of W m^{-2}.

$$LE = R_n - G - H \tag{1}$$

The method for calculating the key components of the surface energy balance in SEBAL has been comprehensively detailed in the works of (Bastiaanssen et al., 1998a, 1998b). Additionally, the application of these calculations within the pySEBAL framework can be found in the research conducted by (Jaafar and Ahmad, 2020; Peddinti and Kisekka, 2022; Xue et al., 2020). Specifically, the net radiation (Rn), which is the actual radiant energy available at the earth's surface, is calculated as the difference between all incoming and outgoing radiant energy flows, as outlined in Eq. (2) by Allen et al. (2007).

$$R_n = [R_{S\downarrow} + R_{L\downarrow}] - [\alpha R_{S\downarrow} + R_{L\uparrow} + (1 - \varepsilon_0) R_{L\downarrow})] \tag{2}$$

where $R_{S\downarrow}$ represents the incoming shortwave solar radiation (W m^{-2}), while $R_{L\downarrow}$ and $R_{L\uparrow}$ denote the incoming and outgoing longwave radiation (W m^{-2}), respectively. The term α refers to the surface albedo, which is a dimensionless coefficient reflecting the proportion of incident light or radiation that is reflected by a surface, and ε_0 is defined as the surface's thermal emissivity (W m^{-2}), indicating its efficiency in emitting thermal radiation.

G quantifies the heat transfer rate into soil through thermal conduction. In the pySEBAL model, G, which is a fraction of the net radiation (Rn), is determined using Eq. (3) based on the empirical equation developed by (Bastiaanssen, 1995).

$$G = T_s(0.0038 + 0.0074\alpha)\left(1 - 0.98NDVI^4\right) \tag{3}$$

where T_s is the surface temperature (K), α is the surface albedo (dimensionless), and $NDVI$ is the Normalized Difference Vegetation Index.

H reflects the heat transferred to the atmosphere through convection and conduction, driven by a temperature gradient between the surface and the air. It is calculated using Eq. (5).

$$H = \frac{\rho_{air} C_p dT}{r_{ah}} \tag{4}$$

where ρ_{air} represents the density of air (Kg m^{-3}), C_p denotes the specific heat capacity of air at constant pressure ($\sim$ 1004 J kg^{-1} K^{-1}), and dT is the temperature difference in the air near the surface for each pixel, and r_{ah} stands for the aerodynamic resistance (s m^{-1}).

Since the exact air temperatures above each individual pixel are not known, dT is deduced by assuming that there is a linear correlation between dT and the altitude-corrected surface temperature. To establish the parameters of this linear correlation, SEBAL employs two reference points known as "anchor" pixels, where the H can be accurately determined. These anchor pixels are identified for every satellite image by selecting the hottest and coldest pixels over the driest part of the landscape and over a moist feature like a water body or an irrigated region, respectively. Once these pixels are selected, pySEBAL calculates the instantaneous latent heat flux (LE) and the Evaporative Fraction (EF) at the instant the satellite data was captured. The daily actual evapotranspiration (ET) is then derived by multiplying EF24 by the total 24-h net radiation, consciously disregarding the relatively insignificant ground heat flux over the course of a day.

$$ET = \frac{8.64 \times 10^7 \times AF \times EF \times (R_{n24} - G_{24})}{\lambda \times \rho_w} \tag{5}$$

where ET represents the daily ET refers to the daily actual evapotranspiration rate (mm d^{-1}) on the date of the aerial imagery overpass λ denotes the latent heat of vaporization (J Kg^{-1}), ρ_w represents the density of water (Kg m^{-3}), AF is the advection factor, R_{n24} indicates the daily average net radiation (W m^{-2}), and G_{24} corresponds to the daily average soil heat flux (W m^{-2}).

2.6. Estimation of gross primary productivity using the VPM model

The Vegetation Photosynthesis Model (VPM) (Xiao et al., 2004) entails the conceptual division of the distribution of photosynthetically active vegetation (PAV) within plant leaves (chloroplasts) and non-photosynthetic vegetation components (such as stems, branches, and cell walls) to estimate the Gross Primary Productivity (GPP) of forests during the active photosynthesis period of vegetation (Xiao et al., 2005). The equation used in the VPM to estimate GPP is given in Eq. (6)

$$GPP = \varepsilon_g \times FAPAR_{PAV} \times PAR \tag{6}$$

where ε_g is the light use efficiency (μmol CO2/μmol PAR), PAR is the photosynthetically active radiation (μmol m^{-2} s^{-1}), and $FAPAR_{PAV}$ is the fraction of PAR absorbed by PAV (chloroplasts).

In the VPM, the parameter ε_g, reflects the light usage efficiency of vegetation and is influenced by various environmental parameters such as temperature, water availability, and the phenological state of the leaves. Each of these factors exerts a regulating effect on ε_g, and they are quantified by specific down-regulation scalars. These scalars, denoted as T_{scalar} for temperature, W_{scalar} for water availability, and P_{scalar} for leaf phenology, serve to modulate the efficiency of light utilization by the vegetation. Incorporating these scalars ε_g can be written as

$$\varepsilon_g = \varepsilon_0 \times T_{scalar} \times W_{scalar} \times P_{scalar} \tag{7}$$

where ε_0 is the maximum light use efficiency, varying at the ecosystem level depending on the specific vegetation type.

The ε_0 value was determined by fitting a nonlinear correlation between net ecosystem exchange (NEE) and incident PAR (Eq. (8)), specifically during the peak of the plant growing season, as described by (Madugundu et al., 2017; Peddinti et al., 2020; Wang et al., 2010; Yan et al., 2009). The calculation was based on an analysis of 30-day (July month data) eddy covariance flux data collected every 30 min during the 2022 growing season. Notably, the ε_0 value for almond orchards was determined in this study to be 0.51 g C^{-mol} PAR.

$$NEE = \frac{\varepsilon_0 \times PAR \times GPP_{max}}{\varepsilon_0 \times PAR + GPP_{max}} - R_{eco} \tag{8}$$

where GPP_{max} is the maximum GPP that was derived from flux data, and R_{eco} is ecosystem respiration.

Temperature plays a crucial role in regulating the rate of photosynthesis, which is the essential biochemical process that allows plants to convert light energy into chemical energy. Understanding this relationship necessitates quantifying the effect of temperature on photosynthesis, which is referred to as the temperature scalar (T_{scalar}). This factor is investigated in the VPM model at each discrete time interval using the Eq. (9) derived by Raich et al. (1991) for a terrestrial ecosystem model.

$$T_{scalar} = \frac{(T - T_{min})(T - T_{\max})}{[(T - T_{min})(T - T_{max})] - (T - T_{opt})^2} \tag{9}$$

where T_{min} represents the lowest temperature at which photosynthetic activities can occur, T_{max} denotes the highest temperature before these processes begin to decline, and T_{opt} is the optimal temperature that allows for peak photosynthetic performance. If the air temperature falls below T_{min}, then T_{scalar} is set to zero.

As the first order of approximation, W_{scalar}, the influence of water on plant photosynthesis is estimated using a satellite-derived water index using Eq. (10)

$$W_{scalar} = \frac{1 + LSWI}{1 + LSWI_{max}} \tag{10}$$

where $LSWI$ Land Surface Water Index, and $LSWI_{max}$ is the maximum value of the LSWI within a peak growth period of almonds considered in this study.

The P_{scalar} is included in the VPM model to account for the influence of leaf age on photosynthesis at the canopy level, and its calculation is dependent on leaf lifetime. The growth cycle in almond orchards is divided into two separate periods. The first phase, which lasts from December to March, is distinguished by the absence of leaves on the trees. This is a dormant stage in which the almond trees preserve energy in preparation for the upcoming bud break, followed by a rapid growth period. In this stage, the influence of leaf maturity on the photosynthetic process throughout the plant canopy is quantified through the application of the P_{scalar} value, as outlined in Eq. (11). The second phase of the orchards begins in late March and lasts through the end of the harvest season in October. To account for the increased photosynthetic activity and robust vegetative development seen during this time, the P_{scalar} was

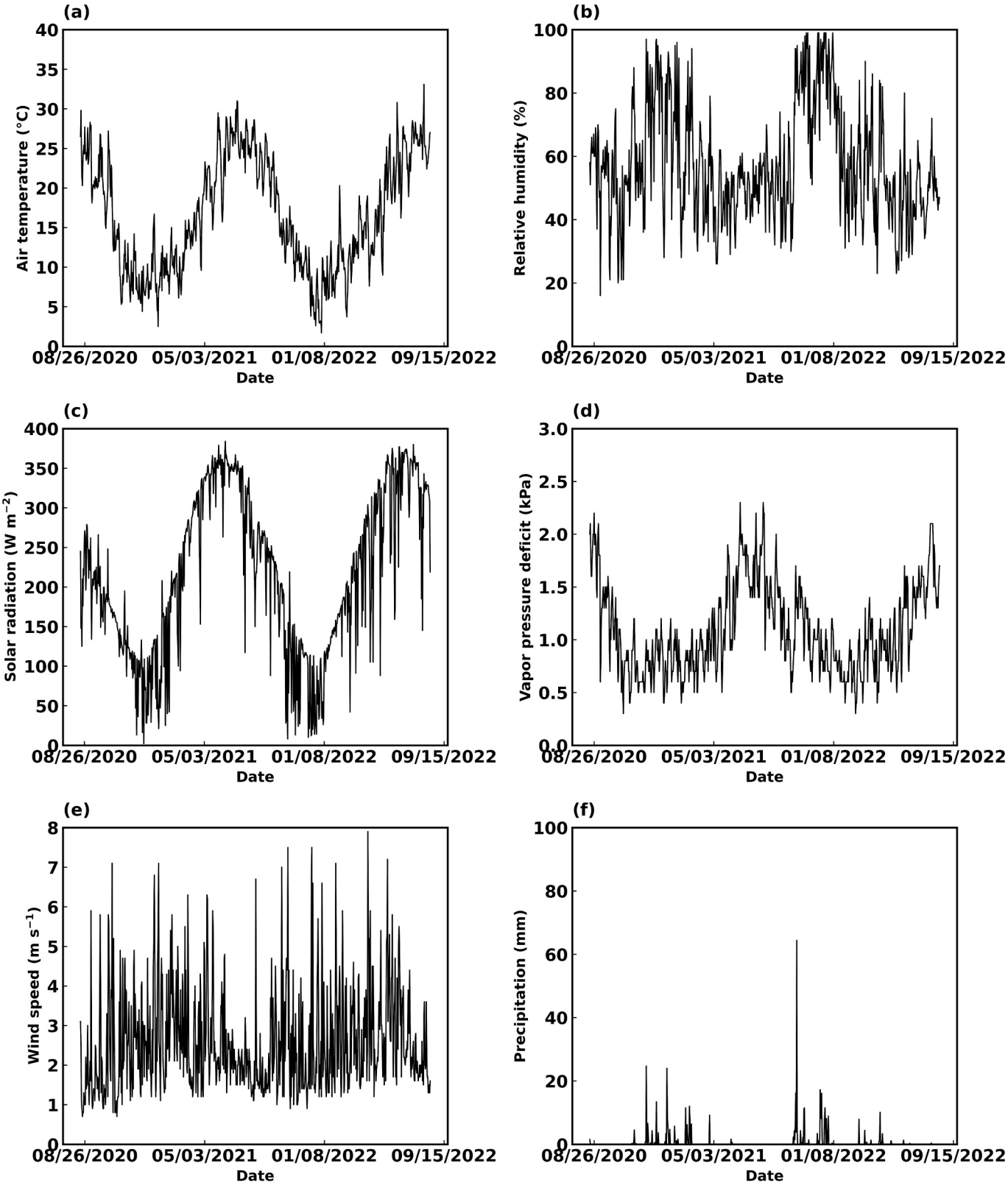


Fig. 3. Environmental conditions during the study period (2020–2022). Daily values of (a) air temperature, (b) relative humidity, (c) solar radiation, (d) vapor pressure deficit, (e) wind speed, and (f) precipitation.

calculated based on Eq. (12).

$$P_{scalar} = \frac{1 + LSWI}{2} \text{ during the dormant stage} \quad (11)$$

$$P_{scalar} = 1 \text{ after leaf full expansion} \quad (12)$$

According to Liu et al. (2018) and (2015), EVI (Enhanced Vegetation Index) based $FAPAR_{PAV}$ calculations have shown effective dependability in analyzing agricultural ecosystems. As a result, utilizing a linear relationship with EVI, calculated $FAPAR_{PAV}$ using Eq. (13). Following the methodology detailed by Xiao et al. (2005) and (2004), the coefficient α was set to 1.0 to simplify parameterization and maintain model consistency.

$$FAPAR_{PAV} = \alpha \times EVI \quad (13)$$

2.7. Estimation of ecosystem water use efficiency

Utilizing satellite data from Landsat, calculations were conducted on a pixel-by-pixel basis to derive WUE based on GPP and ET values. By applying these algebraic operations in accordance with Eq. (13), the ability to map and understand spatial variations in WUE across different parts of the orchard was facilitated, correlating these differences with resource availability and agricultural practices. To confirm the reliability of this satellite-based approach, an assessment of its accuracy was conducted by evaluating the fit of statistical residual parameters within the flux tower footprint. Subsequently, the investigation into WUE over time was undertaken to identify and explain patterns of change within individual seasons and across different seasons.

$$WUE = \frac{GPP}{ET} \quad (14)$$

3. Results

3.1. Environmental variables dynamics

The three-year study period (2020−2022) exhibited distinct seasonal and interannual variations in environmental conditions that influenced carbon and water fluxes in the almond orchard (Fig. 3). Daily average air temperature followed a characteristic Mediterranean climate pattern, ranging from 3 °C during winter months (December–February) to 30 °C during summer (June–August). The seasonal temperature amplitude remained relatively consistent across years, though 2021 experienced slightly higher peak summer temperatures compared to 2020 and 2022 (Fig. 3a). Relative humidity exhibited substantial seasonal fluctuations, ranging from 25 % to 95 % throughout the study period (Fig. 3b). During the growing summer season (June–September), relative humidity typically ranged from 25 % to 55 %, reflecting the characteristic dry conditions of California's Mediterranean summer. In contrast, winter months showed higher humidity (60–95 %) associated with the rainy season. Interannual comparison revealed that 2020 experienced lower average humidity during summer months compared to subsequent years, potentially increasing evaporative demand during this period.

Solar radiation followed a clear seasonal pattern with maximum values occurring during summer months (Fig. 3c). Daily average radiation ranged from 5 W m^{-2} during winter to 400 W m^{-2} during summer, with peak values consistently observed in June and July. The 2022 growing season exhibited greater variability in radiation compared to previous years, with more frequent fluctuations likely due to increased cloud cover events. These radiation patterns directly influenced photosynthetic activity and evaporative demand throughout the orchard. Vapor pressure deficit (VPD), a key driver of transpiration, showed pronounced seasonal dynamics with values ranging from 0.5 to 2.2 kPa across the study period (Fig. 3d). Peak VPD values occurred during summer months (May–September), reaching maximum values between 1.5 and 2.2 kPa, indicating strong atmospheric demand for water during the primary growing season. Notably, 2021 experienced higher peak VPD values compared to other years, potentially increasing water stress during critical fruit development stages.

Wind speed ranged from 1 to 7 m s^{-1} throughout the study period, with a distinct seasonal pattern of lower wind speeds during summer months (Fig. 3e). From June to September, minimum values typically ranged from 1 to 2.5 m s^{-1}, while other months exhibited greater variability and higher average wind speeds. This seasonal wind pattern influences boundary layer conductance and consequently affects both carbon uptake and water loss from the orchard canopy. Precipitation showed substantial interannual variability across the study period (Fig. 3f). The 2020 water year was exceptionally dry, with total recorded rainfall of only 48 mm. In contrast, 2021 received significantly higher precipitation (383 mm), primarily concentrated during winter months. The 2022 water year returned to dry conditions with only 36 mm of precipitation. This precipitation variability created different baseline soil moisture conditions across years, though irrigation remained the primary water source throughout the growing seasons due to the Mediterranean climate's characteristic summer drought. These environmental conditions collectively established the meteorological context for carbon and water fluxes in the almond orchard, with their seasonal and interannual variations driving the observed patterns in GPP, ET, and WUE described in subsequent sections.

3.2. Seasonal dynamics of carbon and water fluxes

3.2.1. Gross primary productivity patterns

Eddy covariance measurements revealed distinct seasonal patterns in gross primary productivity (GPP) that closely followed the phenological cycle of almond trees (Fig. 4a). Daily GPP values ranged from 0.5 to 11.5 g C m^{-2} d^{-1} across the three-year study period, with a clear annual cycle that reflected the deciduous nature of almond trees and their characteristic Mediterranean-climate adaptation. During the dormant season (November–February), when almond trees shed their leaves and enter physiological dormancy, GPP values were consistently low, ranging from 0.5 to 3 g C $m^{-2}d^{-1}$. This residual carbon uptake during dormancy likely originated from limited photosynthesis in evergreen cover crops and orchard floor vegetation rather than the almond trees themselves. As temperatures increased in late February and early March, almond trees transitioned from dormancy to bud break and flowering, initiating a rapid increase in ecosystem carbon uptake. The spring transition period (March–April) showed a steep increase in GPP as leaf development progressed, and canopy photosynthetic capacity expanded. By late April, GPP typically reached 6–8 g C $m^{-2}d^{-1}$, reflecting the establishment of full canopy conditions.

Peak GPP values (10–11.5 g C $m^{-2}d^{-1}$) were consistently observed during the summer months (June–August), coinciding with the fruit development stage when almond trees allocate substantial resources to nut growth and maturation. During this period, the fully developed canopy maximized light interception while favorable temperature conditions supported high photosynthetic rates. Interannual comparison revealed that 2022 exhibited slightly higher peak GPP values compared to previous years, potentially reflecting optimized orchard management practices or favorable microclimatic conditions. Following harvest in late August to early September, GPP began a gradual decline as trees reduced photosynthetic activity and prepared for leaf senescence. This post-harvest decline was more pronounced than the spring increase, with GPP decreasing from peak values to dormancy levels over approximately 8–10 weeks. By November, GPP had returned to dormant-season levels as trees completed leaf drop and entered winter dormancy. The VPM model successfully captured these seasonal GPP dynamics, as evidenced by the strong agreement between model estimates and tower measurements (Fig. 4b). Linear regression analysis of VPM-derived GPP against EC-measured GPP yielded an R^2 of 0.88 and RMSE of 1.5 g C m^{-2} d^{-1}, indicating robust model performance across the range of observed values. The model slightly underestimated peak

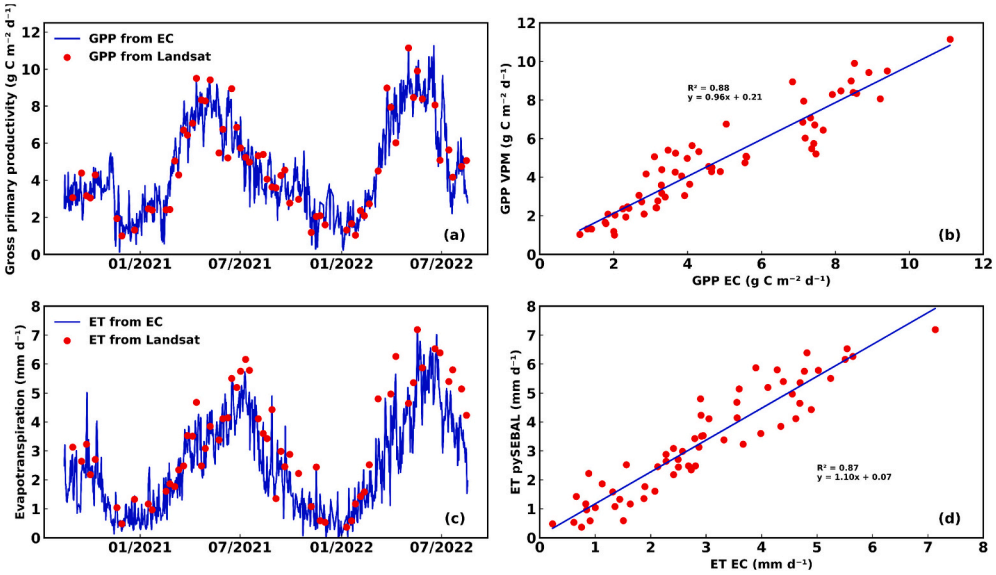


Fig. 4. Seasonal dynamics in daily gross primary production (GPP) (a) and evapotranspiration (ET) (b) as recorded by an eddy covariance flux tower. In addition, the vegetation photosynthetic model (VPM) produced GPP values and pySEBAL-derived ET values are displayed as red dots over the Landsat overpass dates for the three years from 2020 to 2022, with their linear regression analysis on the right panels.

summer GPP in some instances, particularly during periods of extremely high temperature, suggesting potential model limitations under environmental extremes.

3.2.2. Evapotranspiration patterns

Evapotranspiration (ET) exhibited seasonal patterns that paralleled GPP dynamics but with distinct differences reflecting the influence of environmental drivers beyond canopy development (Fig. 4c). Daily ET values ranged from 0.5 to 7.5 mm d^{-1} across the study period, with seasonal amplitude modulated by both biological factors (phenology, canopy development) and physical factors (radiation, temperature, VPD). During the dormant season (November–February), ET rates were consistently low (< 2 mm d^{-1}), reflecting minimal transpiration from leafless almond trees and reduced evaporative demand due to lower temperatures and radiation. Despite low biological activity during this period, ET showed greater day-to-day variability than GPP, responding more directly to fluctuations in meteorological conditions such as wind events and winter rainfall. As almond trees progressed through bud break and flowering in March, ET began to increase in parallel with GPP, though the rate of increase was initially less steep. This pattern suggests that early-season carbon uptake increased more rapidly than water use, potentially reflecting favorable water use efficiency during leaf development when transpiring leaf area was still expanding but photosynthetic capacity was already substantial.

ET reached maximum values (6–7.5 mm d^{-1}) during summer months (June–August), coinciding with peak GPP but also with maximum solar radiation, temperature, and VPD. The highest daily ET values were typically observed in July, when the combination of full canopy development and maximum atmospheric demand created optimal conditions for water flux. Interannual comparison revealed that peak ET values were similar across years despite differences in precipitation, highlighting the dominant role of irrigation in maintaining consistent water availability during the growing season. Post-harvest ET decline followed a pattern similar to GPP but with a slightly more gradual decrease, particularly in the early post-harvest period (September–October). This pattern suggests that transpiration continued at relatively high rates even as photosynthetic activity began to decrease, potentially reflecting a decoupling of carbon and water fluxes during the transition to dormancy. The pySEBAL model effectively captured these seasonal ET dynamics, with strong agreement between model estimates and tower measurements (Fig. 4d). Linear regression analysis yielded an R^2 of 0.87 and RMSE of 0.9 mm d^{-1}, indicating robust model performance across the range of observed values. The model showed a slight tendency to overestimate ET under very high evaporative demand conditions, possibly due to limitations in capturing stomatal regulation under extreme VPD.

3.2.3. Water use efficiency dynamics

Ecosystem water use efficiency (WUE), calculated as the ratio of GPP to ET, exhibited complex seasonal patterns that reflected the differential responses of carbon and water fluxes to environmental conditions and phenological stages (Fig. 5a). Daily WUE values ranged from 0.5 to 5.9 g C $kg^{-1}H_2O$ across the study period, with an average of 2.14 g C $kg^{-1}H_2O$. The seasonal WUE pattern revealed distinct phases corresponding to key phenological transitions in the almond orchard. During the dormant season (November–February), WUE exhibited high variability with values ranging from 1.5 to 6 g C $kg^{-1}H_2O$. This variability during dormancy reflects the complex balance between minimal but fluctuating carbon uptake (primarily from orchard floor vegetation) and low but environmentally responsive evaporation. The highest WUE values of the entire annual cycle were occasionally observed during this dormant period, particularly on days with favorable temperature and humidity conditions that supported photosynthesis while limiting evaporative water loss. As trees transitioned from dormancy to flowering and leaf development (March–April), WUE showed a decreasing trend with values dropping below 4 g C $kg^{-1}H_2O$. This decrease occurred despite rising GPP, indicating that water use increased proportionally faster than carbon uptake during this phenological transition. The declining WUE during bloom likely reflects the substantial water requirements for reproductive development and initial leaf expansion, processes that consume water but do not immediately translate to maximum photosynthetic returns.

During the kernel development and maturation phase (May–August), WUE values remained relatively low (1–4 g C $kg^{-1}H_2O$) despite peak GPP, reflecting the high-water requirements for fruit development and the strong evaporative demand during summer months. WUE reached minimum values (as low as 0.5 g C $kg^{-1}H_2O$) by late August, coinciding with the completion of nut maturation and the onset of harvest. This seasonal minimum in WUE indicates that water use remains high even as carbon uptake begins to decline at the end of the fruit development

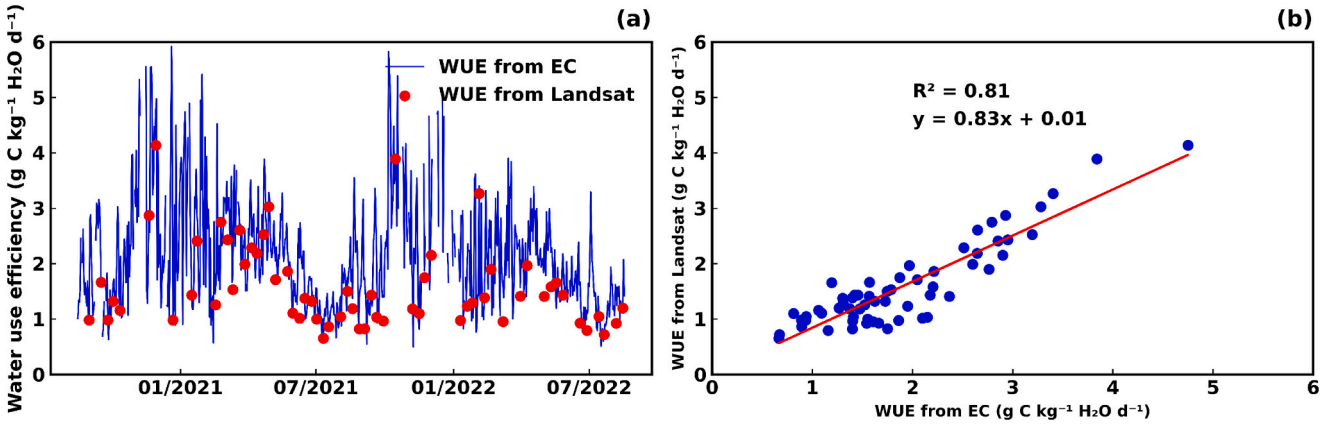


Fig. 5. Seasonal fluctuations in daily water use efficiency (WUE) were derived from eddy covariance flux tower data (a) and analyzed through regression (b) between EC and Landsat-derived WUE in almond orchards for the three years spanning from 2020 to 2022.

cycle. Post-harvest (September–October), WUE exhibited a sharp decrease followed by a gradual recovery as trees transitioned toward dormancy. This pattern suggests complex post-harvest physiology, where initial reductions in photosynthetic activity occur while transpiration continues, followed by a more balanced reduction in both fluxes as leaf senescence progresses. Interannual comparison revealed consistent seasonal WUE patterns across the years despite differences in environmental conditions, indicating that these efficiency dynamics are strongly governed by phenological controls. However, subtle differences were observed, particularly during the 2021 growing season, which showed slightly lower mid-summer WUE compared to other years, potentially reflecting the impact of higher VPD conditions during this period. The remote sensing approach successfully captured these WUE dynamics, as evidenced by the strong agreement between satellite-derived and tower-based WUE estimates (Fig. 5b). Linear regression analysis yielded an R^2 of 0.81, indicating that the integrated VPM-

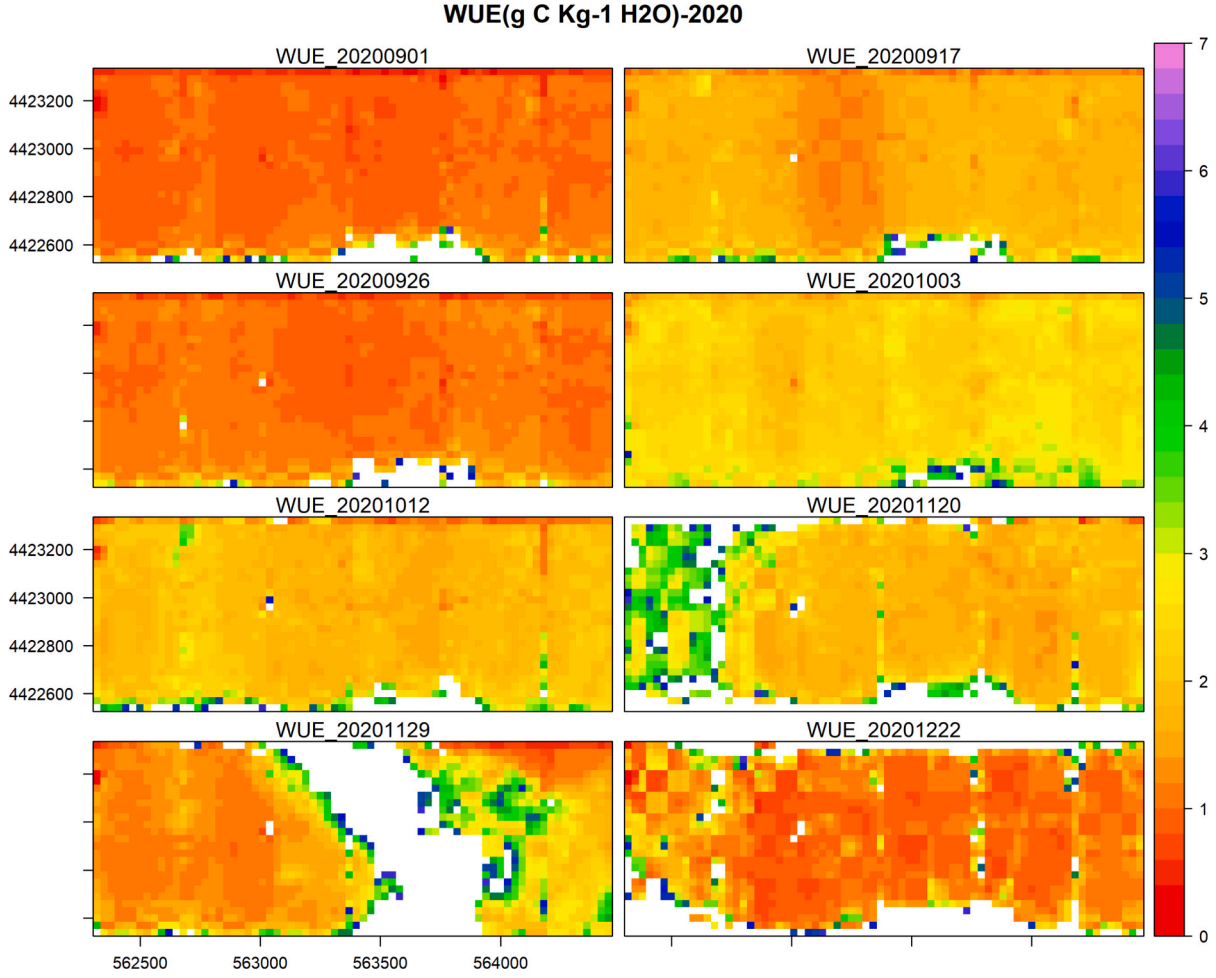


Fig. 6a. Spatial distribution of WUE fluxes was calculated from Landsat imagery for the dates of satellite overpasses during the year 2020. The white pixels indicate that there is no data.

pySEBAL approach effectively represented the temporal variations in ecosystem WUE. This validation provides confidence in the spatial WUE patterns derived from satellite observations.

3.3. Spatial patterns of water use efficiency

Spatial patterns of WUE in almond orchards demonstrated distinct spatial and temporal variations from 2020 to 2022, closely associated with specific phenological stages (Figs. 6a–6c). During the dormant season (November–February), spatial WUE values generally ranged from approximately 2 to 4 g C $kg^{-1}H_2O$, with consistently higher efficiency observed in central and northern orchard sections. Peripheral orchard areas displayed comparatively lower WUE values (1–2 g C $kg^{-1}H_2O$), potentially indicating variability in soil moisture or localized environmental conditions. Throughout the leaf development phase (March–April), spatial WUE values notably decreased, generally falling below 2 g C $kg^{-1}H_2O$ across most orchard areas. This reduction was particularly evident along southern and eastern orchard boundaries, likely reflecting increased water demand for foliage expansion and flowering. Central orchard zones retained marginally higher values (around 2 g C $kg^{-1}H_2O$), indicating slightly better water use efficiency during these critical phenological transitions.

During the kernel maturation phase (May–August), spatial WUE consistently remained low, ranging from 0.5 to 2 g C $kg^{-1}H_2O$. Minimal spatial differences were observed, indicating uniformly high-water use across the orchard associated with fruit development and elevated summer evaporative demand. However, occasional localized pockets within central orchard regions exhibited marginally higher WUE values, suggesting spatial heterogeneity in water use, possibly driven by differential irrigation management practices or soil characteristics. Post-harvest periods (September–October) showed gradual spatial recovery in WUE values, generally rising to approximately 2–3 g C $kg^{-1}H_2O$, particularly prominent in central orchard zones. Peripheral orchard sections continued to exhibit lower efficiency, maintaining values below 2 g C $kg^{-1}H_2O$, reflecting ongoing spatial variability in water availability or residual physiological stress from preceding growth phases.

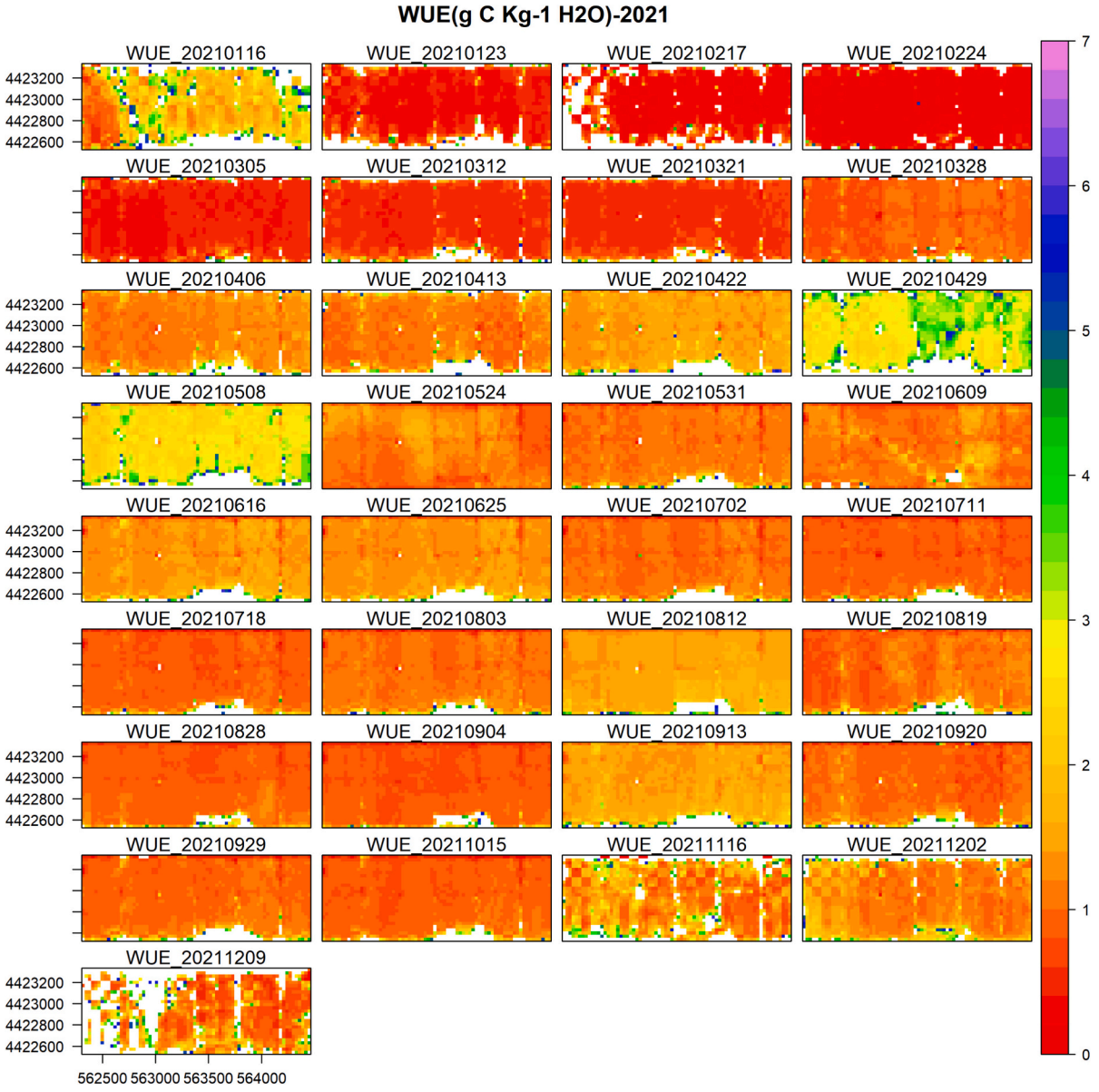


Fig. 6b. Spatial distribution of WUE fluxes was calculated from Landsat imagery for the dates of satellite overpasses during the year 2021. The white pixels indicate that there is no data.

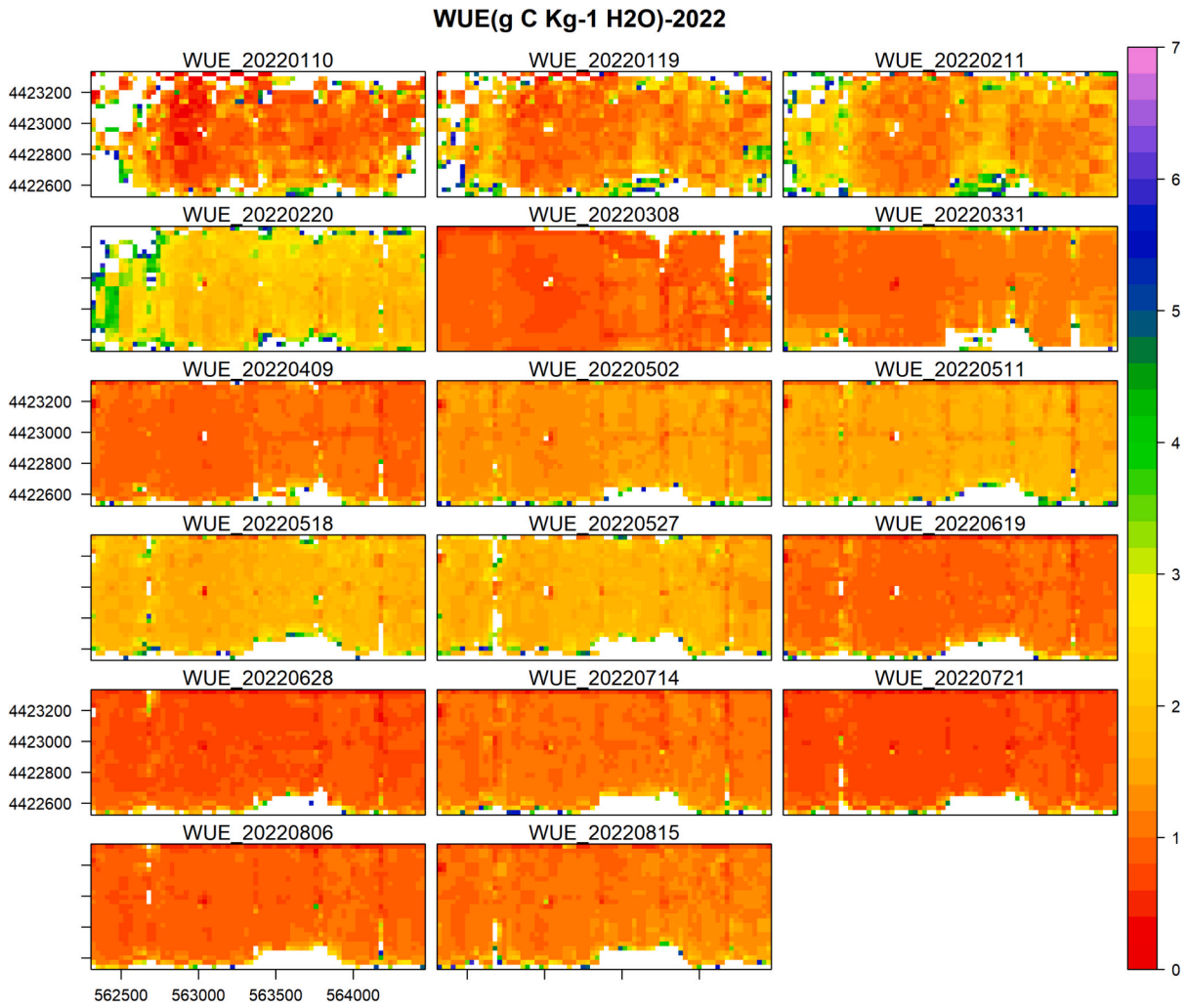


Fig. 6c. Spatial distribution of WUE fluxes was calculated from Landsat imagery for the dates of satellite overpasses during the year 2022. The white pixels indicate that there is no data.

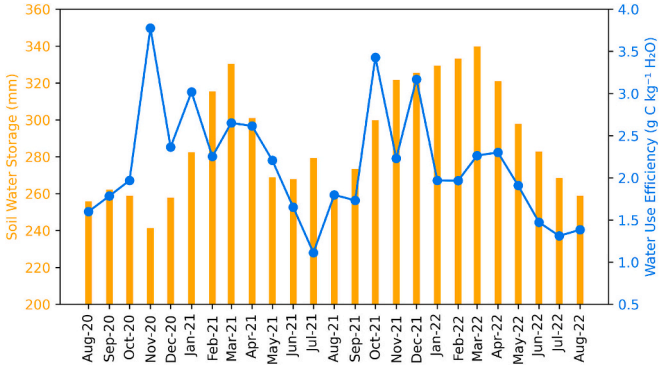


Fig. 7. Monthly variation of root-zone soil water storage (76 cm) and water use efficiency in an almond orchard from 2020 to 2022.

3.4. Seasonal dynamics of soil water storage and water use efficiency

Fig. 7 illustrates the seasonal variation of soil water storage (SWS) and WUE in an almond orchard, with SWS calculated across the root zone depth of 76 cm. During the growth period, spanning from approximately March to August, SWS values are notably lower compared to other periods, likely due to the increased water uptake by the almond trees to support their active growth and development. Concurrently, the WUE values are also low, which may reflect a higher proportion of water loss through transpiration and evaporation relative to carbon assimilation, possibly influenced by the trees' high-water demand and environmental factors such as temperature and solar radiation. In contrast, from November to February, SWS values rise significantly, suggesting reduced root water uptake and lower transpiration rates due to the dormant phase of the almond trees during the colder months. This period also exhibits higher WUE values, indicating that the limited water use is more efficiently converted into biomass, as the trees' physiological activities are minimized. These observations underscore the seasonal interplay between water availability, tree physiology, and environmental conditions throughout the year, providing a comprehensive view of water dynamics across the almond crop cycle.

3.5. Environmental controls on water use efficiency

The relationships between environmental variables and ecosystem fluxes (GPP and ET) were analyzed at monthly time scales, revealing distinct patterns of influence on WUE. Figs. 8 and 9 present these relationships for the almond orchard over the three-year study period (2020–2022). Precipitation showed weak negative relationships with both monthly GPP ($R^2 = 0.04$) and ET ($R^2 = 0.16$) (Fig. 8a). Despite these weak negative relationships with individual fluxes, precipitation exhibited a moderate positive relationship with WUE ($R^2 = 0.42$), with

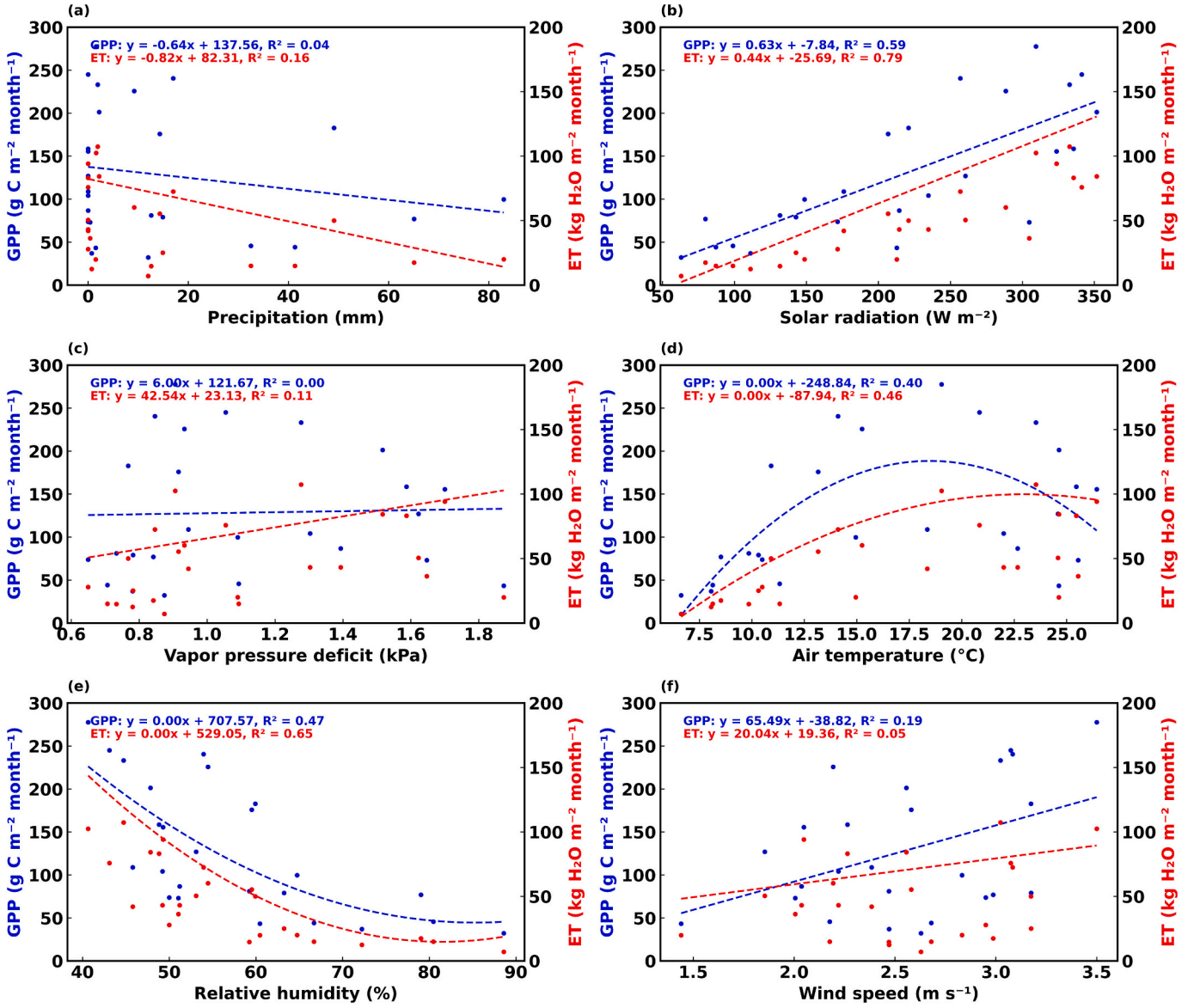


Fig. 8. Relationship between monthly GPP (left axis) and Evapotranspiration (right axis) with monthly accumulation of (a) precipitation, and averages of (b) solar radiation, (c) vapor pressure deficit, (d) air temperature, (e) relative humidity, and (f) wind speed for the almond orchard over three years from 2020 to 2022. The regression lines in blue represent GPP and the lines in red represent evapotranspiration.

WUE increasing by approximately 0.02 g C $kg^{-1}H_2O$ per mm of precipitation (Fig. 9a). This positive relationship suggests that precipitation events may have proportionally greater negative effects on ET than on GPP, potentially due to reduced atmospheric demand and increased soil moisture availability during and after rainfall events.

Solar radiation showed strong positive relationships with both GPP ($R^2 = 0.59$) and ET ($R^2 = 0.79$) (Fig. 8b). Both fluxes increased linearly with increasing radiation, reflecting the fundamental role of solar energy in driving both photosynthesis and evapotranspiration. However, the steeper slope for GPP compared to ET resulted in a negative relationship between solar radiation and WUE ($R^2 = 0.40$) (Fig. 9b). This pattern indicates that under high radiation conditions, the proportional increase in ET exceeds that of GPP, reducing overall water use efficiency. Vapor pressure deficit (VPD) showed no significant relationship with GPP ($R^2 = 0.00$) but a moderate positive relationship with ET ($R^2 = 0.11$) (Fig. 8c). The lack of GPP response to VPD coupled with increasing ET at higher VPD values resulted in a moderate negative relationship between VPD and WUE ($R^2 = 0.44$), with WUE decreasing by approximately 1.20 g C $kg^{-1}H_2O$ per kPa increase in VPD (Fig. 9c). This pattern reflects the direct influence of atmospheric water demand on transpiration rates while photosynthesis remains relatively unaffected within the observed VPD range.

Air temperature exhibited non-linear relationships with both GPP and ET (Fig. 8d). GPP showed a quadratic response to temperature ($R^2 = 0.40$), increasing up to approximately 17.5 °C and then declining at higher temperatures. ET showed a similar but less pronounced quadratic pattern ($R^2 = 0.46$). The resulting relationship between temperature and WUE was also non-linear ($R^2 = 0.58$) providing the best fit (Fig. 9d). WUE remained relatively stable at temperatures between 7.5 °C and 15 °C, then declined more rapidly as temperatures increased above 20 °C. This pattern suggests that high temperatures disproportionately reduce photosynthesis compared to transpiration, likely due to increased photorespiration and potential stomatal closure at high temperatures. Relative humidity showed strong negative relationships with both GPP ($R^2 = 0.47$) and ET ($R^2 = 0.65$), with both fluxes decreasing non-linearly as humidity increased (Fig. 8e). Despite both fluxes decreasing with increasing humidity, WUE showed a moderate positive linear relationship with relative humidity ($R^2 = 0.32$), with WUE

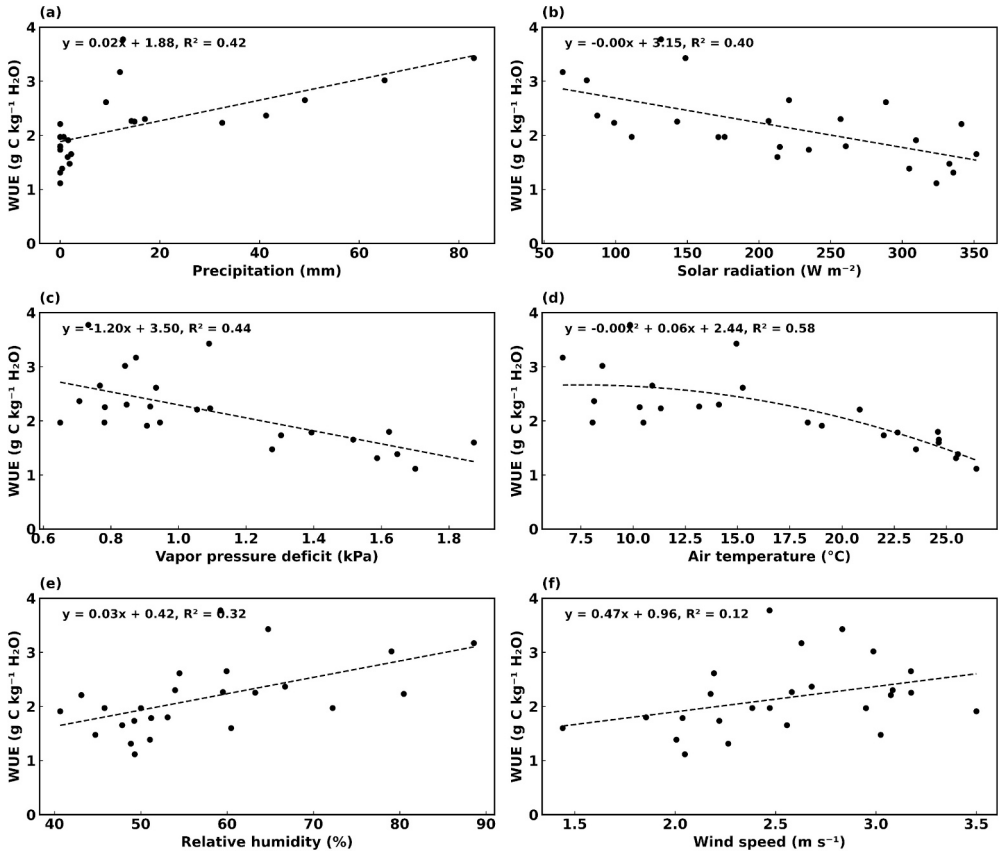


Fig. 9. Relationship between monthly average water use efficiency (left axis) with monthly accumulation of (a) precipitation, and averages of (b) solar radiation, (c) vapor pressure deficit, (d) air temperature, (e) relative humidity, and (f) wind speed for the almond orchard over three years from 2020 to 2022.

increasing by approximately 0.03 g C $kg^{-1}H_2O$ per percentage point increase in humidity (Fig. 9e). This pattern is consistent with the negative VPD-WUE relationship, as relative humidity and VPD are inversely related. The positive relationship suggests that under high humidity conditions, the reduction in ET outpaces the reduction in GPP, resulting in more efficient water use. Wind speed showed weak positive relationships with both GPP ($R^2 = 0.19$) and ET ($R^2 = 0.05$) (Fig. 8f). The relationship between wind speed and WUE was also positive but weak ($R^2 = 0.12$), with WUE increasing by approximately 0.47 g C $kg^{-1}H_2O$ per m s^{-1} increase in wind speed (Fig. 9f). This positive relationship, though weak, suggests that increased air movement may enhance carbon uptake more than water loss, potentially by reducing boundary layer resistance and improving CO_2 diffusion to photosynthetic tissues. The relative importance of environmental variables in explaining WUE variation, as assessed by the coefficient of determination (R^2), ranked as follows: air temperature ($R^2 = 0.58$), vapor pressure deficit ($R^2 = 0.44$), precipitation ($R^2 = 0.42$), solar radiation ($R^2 = 0.40$), relative humidity ($R^2 = 0.32$), and wind speed ($R^2 = 0.12$). This ranking highlights the dominant role of temperature in controlling WUE in almond orchards, followed by atmospheric water demand (VPD) and water availability (precipitation).

4. Discussion

Integrating eddy covariance and remote sensing data has delineated distinct water use efficiency (WUE) patterns in almond orchards, diverging from those observed in other ecosystems. These patterns arise from the trees' complete winter dormancy, early spring flowering under potential water deficit, rapid and highly synchronized nut development, adaptation to Mediterranean climatic conditions, and intensive management practices including high-density planting, precision fertigation, and phenology-based pruning (Álvarez et al., 2020; Esparza et al., 2001). Elucidating these mechanistic drivers yields critical insights for optimizing water management in this economically significant perennial agroecosystem. The observed pattern of high WUE during dormancy, declining efficiency during bloom and leaf development, minimum efficiency during kernel filling, and recovery during post-harvest differs substantially from patterns reported in evergreen systems (Liu et al., 2017; Wu et al., 2015) and annual crops (Tong et al., 2009). This distinctive phenological control can be explained by the resource allocation strategy of almond trees (Kandhway et al., 2025).

During dormancy, minimal physiological activity and leafless canopies result in low absolute fluxes of both carbon and water, but the limited photosynthesis from orchard floor vegetation can occur at relatively high efficiency due to cool, humid winter conditions (Sperling et al., 2025). As trees transition to flowering and leaf development in spring, they prioritize reproductive structures and rapid canopy expansion, processes that require substantial water investment before full photosynthetic capacity is established (Sperling et al., 2025; Trainin et al., 2022). This temporal mismatch between water use and carbon gain explains the declining WUE during this critical phenological transition. The minimum WUE observed during kernel filling (June–August) reflects the high-water requirements for fruit development combined with increasing atmospheric demand (Moldero et al., 2021). During this period, almond trees maintain high transpiration rates to support carbohydrate translocation to developing nuts and to regulate canopy temperature under hot summer conditions. This physiological prioritization of reproductive development and thermal regulation over water conservation represents an evolutionary adaptation to the Mediterranean climate and has been reinforced through selective breeding for high yield. The post-harvest recovery in WUE indicates a shift in resource allocation from fruit production to reserve accumulation and

preparation for dormancy. During this period, trees maintain photosynthetic activity while gradually reducing transpiration as environmental demand decreases and leaf senescence begins (Egea et al., 2010; Espadafor et al., 2017). This transition represents a critical period for tree health and subsequent year productivity, as carbon reserves accumulated during this time support initial growth in the following spring.

The seasonal WUE dynamics in almond orchards differ substantially from patterns reported in natural forest ecosystems. In evergreen forests, Liu et al. (2017) observed relatively stable WUE throughout the year with modest seasonal variations driven primarily by environmental conditions rather than phenology. In contrast, our almond orchard exhibited pronounced seasonal WUE fluctuations strongly linked to phenological transitions, reflecting the deciduous nature of these trees and their agricultural management. The environmental responses of WUE also showed important differences. While both systems exhibited negative relationships between WUE and VPD, the sensitivity to VPD was greater in the almond orchard, likely reflecting differences in stomatal regulation strategies. Natural forests often show more conservative stomatal behavior under high VPD, prioritizing water conservation over maximum carbon gain. In contrast, irrigated almond orchards maintain higher stomatal conductance under elevated VPD, maximizing productivity at the expense of efficiency (Espadafor et al., 2017). Compared to annual crops, almond orchards showed both similarities and distinctive differences in WUE patterns. Tong et al. (2009) reported that irrigated wheat-maize rotation systems exhibited maximum WUE during grain filling stages, contrasting with the minimum efficiency we observed during almond kernel development. This difference likely reflects the contrasting resource allocation strategies of annual and perennial crops (Chapman et al., 2022). Annual crops maximize efficiency during reproductive stages to complete their life cycle within a single season, while perennial trees like almonds prioritize long-term survival and multi-year reproduction, allowing for periods of lower efficiency when necessary for reproductive success (Lindberg et al., 2020; Sperling et al., 2023).

Our findings align with and extend recent research on WUE in tree crop systems. Kandhway et al. (2025) conducted a simulation-based study in California examining how elevated CO_2 and warming could impact water use and phenology in almond and pistachio orchards. Their model projected a modest increase in almond WUE under elevated CO_2, partially offsetting rising evapotranspiration demands due to warming. While their study used process-based modeling, our empirical results derived from EC and remote sensing highlight how phenological shifts and atmospheric conditions drive seasonal WUE variation in mature orchards. The agreement between their projected responses and our observed WUE minima during kernel filling underscores the importance of both physiological and environmental controls in WUE dynamics. Complementing our field-based approach, Álvarez et al. (2023) conducted a controlled greenhouse experiment in Spain evaluating WUE among four almond cultivars grafted onto the dwarfing rootstock 'Rootpac-20'. They reported significant genotypic variation in WUE, with some cultivars showing superior efficiency under uniform irrigation. In contrast, our field-based study in California demonstrates that even under standardized commercial conditions, seasonal WUE patterns are primarily driven by phenology and environmental stressors like VPD, rather than cultivar differences. Together, these studies suggest that optimizing WUE in almond orchards requires a dual focus on both cultivar selection and dynamic, phenology-aware irrigation strategies. The importance of orchard structure and development stage on WUE was highlighted by Thorp et al. (2023), who examined WUE in young high-density almond orchards in South Australia. Their research showed that WUE (measured as liters per gram of kernel yield) remained consistent across planting densities when per-tree irrigation volumes were matched. Their work emphasizes structural factors such as age, spacing, and early growth irrigation strategy. In contrast, our study in mature California orchards highlights how WUE varies seasonally due to phenological development and environmental demand. The two studies together reveal that improving WUE across an orchard's lifespan requires stage-specific strategies—structural and developmental considerations during establishment and phenological, environmental alignment in mature phases.

Comparisons with other tree crop systems provide additional context for our findings. Peddinti et al. (2020) reported that citrus orchards in India exhibited maximum WUE during the cool, dry season and minimum efficiency during the hot, humid monsoon period. While this seasonal pattern superficially resembles our observations in almonds, the underlying mechanisms differ. In citrus, the seasonal WUE pattern was driven primarily by environmental conditions, with high humidity during monsoon reducing the atmospheric demand gradient for transpiration. In contrast, almond WUE dynamics were strongly influenced by phenological transitions, reflecting the deciduous nature of these trees compared to evergreen citrus. This distinction highlights the importance of considering both environmental and phenological factors when developing water management strategies for different orchard systems. Irrigation management approaches also significantly impact WUE in tree crops, as demonstrated by Stagno et al. (2024) who evaluated the impact of three deficit irrigation strategies such as SSDI, RDI, and PRD on WUE in orange orchards in Sicily, Italy. All treatments improved WUE without reducing fruit yield, with PRD saving up to 49 % of irrigation water. While their study focuses on evergreen citrus and irrigation methods, our findings in deciduous almond orchards highlight phenological controls on WUE, especially the post-harvest recovery period, which aligns conceptually with their observed nutrient allocation benefits under PRD. These parallels reinforce the importance of both physiological timing and irrigation strategy in optimizing WUE across diverse woody crops.

The relationship between irrigation levels and WUE has been explored in various tree crop systems. da Silva et al. (2009) quantified mango orchard WUE under four irrigation levels in semiarid northeastern Brazil, showing maximum WUE at 70 % and 80 % of ETo. Their results confirmed that moderate water deficits can enhance WUE, consistent with deficit irrigation studies in Mediterranean climates. Unlike their empirical water balance approach focusing on applied irrigation, our eddy covariance–based method quantifies seasonal WUE dynamics as influenced by phenology and atmospheric demand, offering complementary insights on optimizing productivity under water-limited conditions. Similarly, Tejero et al. (2011) compared sustained, regulated, and low-frequency deficit irrigation strategies in citrus orchards in southwestern Spain and found that all improved agricultural and financial WUE without yield penalties. Their use of stem water potential to guide irrigation aligns with the physiological underpinnings of our almond WUE patterns, particularly in periods of reproductive stress. While their work emphasizes irrigation scheduling, our study contributes a complementary phenology-based framework for WUE optimization in deciduous systems under Mediterranean climates.

Broader perspectives on WUE improvement strategies provide valuable context for our findings. Cooper et al. (1987) reviewed WUE improvement strategies for annual crops under rainfed systems in West Asia and North Africa. They identified three mechanistic pathways to increase WUE improving transpiration efficiency, maximizing transpiration over evaporation, and extending the effective growing season. While focused on annual cereals and legumes, their principles translate to our almond findings: particularly the importance of managing periods of low photosynthetic return (e.g., early leaf-out, post-harvest) to avoid WUE inefficiencies. Our data affirm the significance of synchronizing carbon gain with water use, even in irrigated perennial systems. The advantages of perennial systems for WUE were demonstrated by Zeri et al. (2013), who used eddy covariance to compare WUE across perennial and annual bioenergy crops in central Illinois. They showed that perennial crops like Miscanthus had higher ecosystem WUE than maize-soy rotations. Their results support our findings that perennial systems with extended growing seasons and efficient canopy development can sustain higher WUE when phenology and carbon allocation are

favorably aligned. The importance of crop specific WUE assessments was emphasized by Katerji et al. (2008), who reviewed WUE data for 16 crops across the Mediterranean basin and identified wide variability due to water regime, crop type, and environmental stress. They stressed the lack of data for fruit trees and emphasized the need for crop-specific, phenology-sensitive WUE assessments. Our study directly addresses this knowledge gap by offering detailed WUE patterns for almonds across developmental stages, supporting their call for precision in Mediterranean WUE research, especially in high-value perennial systems.

These findings underscore the importance of phenological monitoring in water management strategies. As climate change alters the timing and intensity of environmental stressors, almond orchards may require adaptive irrigation scheduling tailored to dynamic WUE patterns. Integrating EC and remote sensing approaches offers a scalable pathway to enhance irrigation efficiency, particularly during phenologically sensitive periods such as flowering and post-harvest reserve accumulation. By understanding the mechanistic basis of seasonal WUE variations, growers can develop targeted irrigation strategies that optimize water use while maintaining productivity and orchard health in this economically important perennial crop system. Building on these insights, future research should investigate long-term climate variability, spatial environmental gradients, management practices, genetic diversity among almond varieties, and contrasting resource allocation strategies between annual and perennial crops collectively influence seasonal and interannual dynamics of water-use efficiency and productivity, using integrated models that combine process-based simulations with remote sensing data.

5. Conclusions

This study underscores the importance of water use efficiency (WUE) as a pivotal ecological indicator for perennial orchard systems in water-limited environments. The integration of eddy covariance measurements with remote sensing provides a robust framework for jointly assessing orchard productivity and water consumption, offering valuable insights to support sustainable resource management in perennial agroecosystems. The multiscale framework applied in this study, which combines ground-based eddy covariance flux observations with satellite-derived estimates, offers robust spatial and temporal insights into crop carbon and water dynamics. This approach enables growers, researchers, and policymakers to refine irrigation management, enhance site-specific decision-making, and strengthen the resilience of high-value specialty crops amid ongoing water scarcity due to regulations or changing climate. Future research can build on these methods by incorporating a wider range of environmental gradients and varietal responses, broadening the application of WUE as an indicator of resource use efficiency and sustainability in orchard systems globally.

CRediT authorship contribution statement

Srinivasa Rao Peddinti: Writing – original draft, Software, Methodology, Formal analysis, Conceptualization. **Isaya Kisekka:** Visualization, Resources, Methodology, Investigation, Funding acquisition, Formal analysis, Conceptualization.

Declaration of competing interest

The authors declare that they have no known competing financial interests or personal relationships that could have appeared to influence the work reported in this paper.

Acknowledgment

This study was supported by the USDA NIFA Specialty Crop Block Grant Program [grant number 180001083SC], the Almond Board of California Grant Project HORT69 Kisekka, and USDA NIFA Award # 2021-68012-35914. We are grateful to the Esteve Ranch management for allowing us to research their farm.

Data availability

Data will be made available on request.

References

Abraha, M., Gelfand, I., Hamilton, S.K., Shao, C., Su, Y.-J., Robertson, G.P., Chen, J., 2016. Ecosystem water-use efficiency of annual corn and perennial grasslands: contributions from land-use history and species composition. Ecosystems 19, 1001–1012. https://doi.org/10.1007/s10021-016-9981-2.

AgNet West, 2024. Almond update: almond acreage in California declines for third straight year [WWW document]. AgNet West. https://agnetwest.com/almond-update-almond-acreage-california-declines-third-straight-year/ (accessed 4.3.25).

Allen, R.G., Tasumi, M., Trezza, R., 2007. Satellite-based energy balance for mapping evapotranspiration with internalized calibration (METRIC)—model. J. Irrig. Drain. Eng. 133, 380–394. https://doi.org/10.1061/(ASCE)0733-9437(2007)133:4(380).

Allen, R.G., Pereira, L.S., Howell, T.A., Jensen, M.E., 2011. Evapotranspiration information reporting: I. Factors governing measurement accuracy. Agric Water Manag 98, 899–920. https://doi.org/10.1016/j.agwat.2010.12.015.

Almond board, 2018. New Research: Water Footprint Smaller for California Almonds Than Global Average [WWW Document]. URL. https://www.almonds.com/almond-industry/industry-news/new-research-water-footprint-smaller-california-almonds-global (accessed 3.12.24).

Álvarez, S., Martín, H., Barajas, E., Rubio, J.A., Vivaldi, G.A., 2020. Rootstock effects on water relations of young almond trees (cv. Soleta) when subjected to water stress and rehydration. Water 12, 3319. https://doi.org/10.3390/w12123319.

Álvarez, S., Núñez, L., Martín, H., Barajas, E., Mirás-Avalos, J.M., 2023. Differences in growth and water use efficiency in four almond varieties grafted onto Rootpac-20. Horticulturae 9, 295. https://doi.org/10.3390/horticulturae9030295.

Bastiaanssen, W.G.M., 1995. Regionalization of Surface Flux Densities and Moisture Indicators in Composite Terrain: A Remote Sensing Approach under Clear Skies in Mediterranean Climates (Ph.D.). PQDT - Global. Wageningen University and Research, Netherlands.

Bastiaanssen, W.G.M., Menenti, M., Feddes, R.A., Holtslag, A.A.M., 1998a. A remote sensing surface energy balance algorithm for land (SEBAL). 1. Formulation. J. Hydrol. 212–213, 198–212. https://doi.org/10.1016/S0022-1694(98)00253-4.

Bastiaanssen, W.G.M., Pelgrum, H., Wang, J., Ma, Y., Moreno, J.F., Roerink, G.J., van der Wal, T., 1998b. A remote sensing surface energy balance algorithm for land (SEBAL).: part 2: validation. J. Hydrol. 212–213, 213–229. https://doi.org/10.1016/S0022-1694(98)00254-6.

Chapman, E.A., Thomsen, H.C., Tulloch, S., Correia, P.M.P., Luo, G., Najafi, J., DeHaan, L.R., Crews, T.E., Olsson, L., Lundquist, P.-O., Westerbergh, A., Pedas, P.R., Knudsen, S., Palmgren, M., 2022. Perennials as future grain crops: opportunities and challenges. Front. Plant Sci. 13, 898769. https://doi.org/10.3389/fpls.2022.898769.

Cooper, P.J.M., Gregory, P.J., Tully, D., Harris, H.C., 1987. Improving water use efficiency of annual crops in the rainfed farming systems of West Asia and North Africa. Exp. Agric. 23, 113–158.

da Silva, V. de P.R., Cunha Campos, J.H.B., de Azevedo, P.V., 2009. Water-use efficiency and evapotranspiration of mango orchard grown in northeastern region of Brazil. Sci. Hortic. 120, 467–472. https://doi.org/10.1016/j.scienta.2008.12.005.

Doll, D., 2017. Almond water requirements. In: Almonds: Botany, Production and Uses, Botany, Production and Uses, pp. 279–290. https://doi.org/10.1079/9781780643540.0279.

Egea, G., Nortes, P.A., González-Real, M.M., Baille, A., Domingo, R., 2010. Agronomic response and water productivity of almond trees under contrasted deficit irrigation regimes. Agric Water Manag 97, 171–181. https://doi.org/10.1016/j.agwat.2009.09.006.

Elfarkh, J., Johansen, K., El Hajj, M.M., Almashharawi, S.K., McCabe, M.F., 2023. Evapotranspiration, gross primary productivity and water use efficiency over a high-density olive orchard using ground and satellite based data. Agric Water Manag 287, 108423. https://doi.org/10.1016/j.agwat.2023.108423.

Espadafor, M., Orgaz, F., Testi, L., Lorite, I.J., González-Dugo, V., Fereres, E., 2017. Responses of transpiration and transpiration efficiency of almond trees to moderate water deficits. Sci. Hortic. 225, 6–14. https://doi.org/10.1016/j.scienta.2017.06.028.

Esparza, G., DeJong, T.M., Weinbaum, S.A., 2001. Effects of irrigation deprivation during the harvest period on nonstructural carbohydrate and nitrogen contents of dormant, mature almond trees. Tree Physiol. 21, 1081–1086.

Evans, R.G., Sadler, E.J., 2008. Methods and technologies to improve efficiency of water use. Water Resour. Res. 44. https://doi.org/10.1029/2007WR006200.

Goodrich, B., 2020. Economic trends in almond production | progressive crop consultant. In: URL. https://progressivecrop.com/2020/04/15/economic-trends-in-almond-production/ (accessed 4.3.25).

Hamilton, S.K., Hussain, M.Z., Bhardwaj, A.K., Basso, B., Robertson, G.P., 2015. Comparative water use by maize, perennial crops, restored prairie, and poplar trees in the US Midwest. Environ. Res. Lett. 10, 064015. https://doi.org/10.1088/1748-9326/10/6/064015.

He, M., Ju, W., Zhou, Y., Chen, J., He, H., Wang, S., Wang, H., Guan, D., Yan, J., Li, Y., Hao, Y., Zhao, F., 2013. Development of a two-leaf light use efficiency model for improving the calculation of terrestrial gross primary productivity. Agric. For. Meteorol. 173, 28–39. https://doi.org/10.1016/j.agrformet.2013.01.003.

Hoover, D.L., Abendroth, L.J., Browning, D.M., Saha, A., Snyder, K., Wagle, P., Witthaus, L., Baffaut, C., Biederman, J.A., Bosch, D.D., Bracho, R., Busch, D., Clark, P., Ellsworth, P., Fay, P.A., Flerchinger, G., Kearney, S., Levers, L., Saliendra, N., Schmer, M., Schomberg, H., Scott, R.L., 2023. Indicators of water use efficiency across diverse agroecosystems and spatiotemporal scales. Sci. Total Environ. 864, 160992. https://doi.org/10.1016/j.scitotenv.2022.160992.

Huang, L., He, B., Han, L., Liu, J., Wang, H., Chen, Z., 2017. A global examination of the response of ecosystem water-use efficiency to drought based on MODIS data. Sci. Total Environ. 1097–1107. https://doi.org/10.1016/j.scitotenv.2017.05.084.

Jaafar, H.H., Ahmad, F.A., 2020. Time series trends of Landsat-based ET using automated calibration in METRIC and SEBAL: the Bekaa Valley, Lebanon. Remote Sens. Environ. 238, 111034. https://doi.org/10.1016/j.rse.2018.12.033.

Kandhway, A., Scarpare, F., Liu, M., Nelson, R., Adam, J.C., Anderson, R.G., Conklin, M. H., Safeeq, M., 2025. Water use dynamics of almond and pistachio crops in the Mediterranean region amid climate change. Agric Water Manag 307, 109219. https://doi.org/10.1016/j.agwat.2024.109219.

Katerji, N., Mastrorilli, M., Rana, G., 2008. Water use efficiency of crops cultivated in the Mediterranean region: review and analysis. Eur. J. Agron. 28, 493–507. https://doi.org/10.1016/j.eja.2007.12.003.

Klein, K., 2024. With already too many almonds, growers could see three billion pounds more of them. KVPR | Valley Public Radio. URL https://www.kvpr.org/local-news/2024-05-17/with-already-too-many-almonds-growers-could-see-three-billion-pounds-more-of-them (accessed 4.3.25).

Kljun, N., Calanca, P., Rotach, M.W., Schmid, H.P., 2015. A simple two-dimensional parameterisation for flux footprint prediction (FFP). Geosci. Model Dev. 8, 3695–3713.

Lindberg, C.L., Hanslin, H.M., Schubert, M., Marcussen, T., Trevaskis, B., Preston, J.C., Fjellheim, S., 2020. Increased above-ground resource allocation is a likely precursor for independent evolutionary origins of annuality in the Pooideae grass subfamily. New Phytol. 228, 318–329. https://doi.org/10.1111/nph.16666.

Liu, Z., Shao, Q., Liu, J., 2015. The performances of MODIS-GPP and -ET products in China and their sensitivity to input data (FPAR/LAI). Remote Sens. (Basel) 7, 135–152. https://doi.org/10.3390/rs70100135.

Liu, X., Chen, X., Li, R., Long, F., Zhang, L., Zhang, Q., Li, J., 2017. Water-use efficiency of an old-growth forest in lower subtropical China. Sci. Rep. 7, 42761. https://doi.org/10.1038/srep42761.

Liu, R., Ren, H., Liu, S., Liu, Q., Yan, B., Gan, F., 2018. Generalized FPAR estimation methods from various satellite sensors and validation. Agric. For. Meteorol. 260–261, 55–72. https://doi.org/10.1016/j.agrformet.2018.05.024.

Liu, X., Feng, X., Fu, B., 2020. Changes in global terrestrial ecosystem water use efficiency are closely related to soil moisture. Sci. Total Environ. 698, 134165. https://doi.org/10.1016/j.scitotenv.2019.134165.

Madugundu, R., Al-Gaadi, K.A., Tola, E., Hassaballa, A.A., Patil, V.C., 2017. Performance of the METRIC model in estimating evapotranspiration fluxes over an irrigated field in Saudi Arabia using Landsat-8 images. Hydrol. Earth Syst. Sci. 21, 6135–6151. https://doi.org/10.5194/hess-21-6135-2017.

Mauder, M., Jung, M., Stoy, P., Nelson, J., Wanner, L., 2024. Energy balance closure at FLUXNET sites revisited. Agric. For. Meteorol. 358, 110235. https://doi.org/10.1016/j.agrformet.2024.110235.

Mei, L., Tong, S., Yin, S., Bao, Y., Huang, X., Alateng, T., Wang, Y., Guo, E., Yuan, Z., Nashun, D., Gao, S., Liu, X., Ye, Z., 2023. Spatiotemporal variations of water use efficiency and its driving factors in Inner Mongolia from 2001 to 2020. J. Geogr. Sci. 33, 169–194. https://doi.org/10.1007/s11442-023-2078-x.

Moldero, D., López-Bernal, Á., Testi, L., Lorite, I.J., Fereres, E., Orgaz, F., 2021. Long-term almond yield response to deficit irrigation. Irrig. Sci. 39, 409–420. https://doi.org/10.1007/s00271-021-00720-8.

Moncrieff, J.B., Massheder, J.M., de Bruin, H., Elbers, J., Friborg, T., Heusinkveld, B., Kabat, P., Scott, S., Soegaard, H., Verhoef, A., 1997. A system to measure surface fluxes of momentum, sensible heat, water vapour and carbon dioxide. J. Hydrol. 188–189, 589–611. https://doi.org/10.1016/S0022-1694(96)03194-0. HAPEX-Sahel.

Muhammad, S., Sanden, B.L., Lampinen, B.D., Smart, D.R., Saa, S., Shackel, K.A., Brown, P.H., 2020. Nutrient storage in the perennial organs of deciduous trees and remobilization in spring – a study in almond (*Prunus dulcis*) (Mill.) D. A. Webb. Front. Plant Sci. 11. https://doi.org/10.3389/fpls.2020.00658.

Niederholzer, F., Ott, J., Jarvis-Shean, K.S., Wheeler-Dykes, B., Pierce, C., Gyawaly, S., Milliron, L., Agyeman, D., Counties, G., Murdock, J., Davis, U., Long, P., Davis, U., Davison, S., Davis, U., Goodrich, B., Davis, U., 2024. Sample costs to establish an orchard and produce almonds.

Norman, J.M., Kustas, W.P., Humes, K.S., 1995. Source approach for estimating soil and vegetation energy fluxes in observations of directional radiometric surface temperature. Agric. For. Meteorol. 77, 263–293. https://doi.org/10.1016/0168-1923(95)02265-Y.

Peddinti, S.R., Kisekka, I., 2022. Estimation of turbulent fluxes over almond orchards using high-resolution aerial imagery with one and two-source energy balance models. Agric Water Manag 269, 107671. https://doi.org/10.1016/j.agwat.2022.107671.

Peddinti, S.R., Kambhammettu, B.V.N.P., Rodda, S.R., Thumaty, K.C., Suradhaniwar, S., 2020. Dynamics of ecosystem water use efficiency in Citrus orchards of Central India using Eddy covariance and Landsat measurements. Ecosystems 23, 511–528. https://doi.org/10.1007/s10021-019-00416-3.

Raich, J.W., Rastetter, E.B., Melillo, J.M., Kicklighter, D.W., Steudler, P.A., Peterson, B. J., Grace, A.L., Moore III, B., Vorosmarty, C.J., 1991. Potential net primary productivity in South America: application of a global model. Ecol. Appl. 1, 399–429. https://doi.org/10.2307/1941899.

Reichstein, M., Falge, E., Baldocchi, D., Papale, D., Aubinet, M., Berbigier, P., Bernhofer, C., Buchmann, N., Gilmanov, T., Granier, A., Grünwald, T., Havránková, K., Ilvesniemi, H., Janous, D., Knohl, A., Laurila, T., Lohila, A., Loustau, D., Matteucci, G., Meyers, T., Miglietta, F., Ourcival, J.-M., Pumpanen, J., Rambal, S., Rotenberg, E., Sanz, M., Tenhunen, J., Seufert, G., Vaccari, F., Vesala, T., Yakir, D., Valentini, R., 2005. On the separation of net ecosystem exchange into assimilation and ecosystem respiration: review and improved algorithm. Glob. Chang. Biol. 11, 1424–1439. https://doi.org/10.1111/j.1365-2486.2005.001002.x.

Sánchez-Navarro, V., Shahrokh, V., Martínez-Martínez, S., Acosta, J.A., Almagro, M., Martínez-Mena, M., Boix-Fayos, C., Díaz-Pereira, E., Zornoza, R., 2022. Perennial alley cropping contributes to decrease soil CO2 and N2O emissions and increase soil carbon sequestration in a Mediterranean almond orchard. Sci. Total Environ. 845, 157225. https://doi.org/10.1016/j.scitotenv.2022.157225.

Soil Survey Staff, S, 1999. A basic system of soil classification for making and interpreting soil surveys. Agric. Handb. 436, 96–105.

Song, Q.-H., Fei, X.-H., Zhang, Y.-P., Sha, L.-Q., Liu, Y.-T., Zhou, W.-J., Wu, C.-S., Lu, Z.-Y., Luo, K., Gao, J.-B., Liu, Y.-H., 2017. Water use efficiency in a primary subtropical evergreen forest in Southwest China. Sci. Rep. 7, 43031. https://doi.org/10.1038/srep43031.

Sperling, O., Gardi, I., Ben-Gal, A., Kamai, T., 2023. Deficit irrigation limits almond trees' photosynthetic productivity and compromises yields. Agric Water Manag 289, 108562. https://doi.org/10.1016/j.agwat.2023.108562.

Sperling, O., Kamai, T., Gardi, I., A Zwieniecki, M., Marino, G., 2025. Modeling tree responses to soil water variability guides irrigation to account for soil winter reserves. Vadose Zone J. 24, e20385. https://doi.org/10.1002/vzj2.20385.

Stagno, F., Brambilla, M., Roccuzzo, G., Assirelli, A., 2024. Water use efficiency in a deficit-irrigated Orange orchard. Horticulturae 10, 498. https://doi.org/10.3390/horticulturae10050498.

Su, Z., 2002. The surface energy balance system (SEBS) for estimation of turbulent heat fluxes. Hydrol. Earth Syst. Sci. 6, 85–100.

Tejero, I.G., Zuazo, V.H.D., Bocanegra, J.A.J., Fernández, J.L.M., 2011. Improved water-use efficiency by deficit-irrigation programmes: implications for saving water in citrus orchards. Sci. Hortic. 128, 274–282. https://doi.org/10.1016/j.scienta.2011.01.035.

Thorp, G., Smith, A., Coates, M., De Bei, R., 2023. Water use efficiency in high density planting trials with almond (Prunus dulcis (mill.) DA Webb). VIII International Symposium on Almonds and Pistachios 1406, 145–152.

Tombesi, S., Lampinen, B.D., Metcalf, S., DeJong, T.M., 2011. Relationships between spur- and orchard-level fruit bearing in almond (Prunus dulcis). Tree Physiol. 31, 1413–1421. https://doi.org/10.1093/treephys/tpr119.

Tong, X.-J., Li, J., Yu, Q., Qin, Z., 2009. Ecosystem water use efficiency in an irrigated cropland in the North China plain. J. Hydrol. 374, 329–337. https://doi.org/10.1016/j.jhydrol.2009.06.030.

Trainin, T., Brukental, H., Shapira, O., Attia, Z., Tiwari, V., Hatib, K., Gal, S., Zemach, H., Belausov, E., Charuvi, D., Holland, D., Azoulay-Shemer, T., 2022. Physiological characterization of the wild almond Prunus arabica stem photosynthetic capability. Front. Plant Sci. 13. https://doi.org/10.3389/fpls.2022.941504.

Turner, D.P., Urbanski, S., Bremer, D., Wofsy, S.C., Meyers, T., Gower, S.T., Gregory, M., 2003. A cross-biome comparison of daily light use efficiency for gross primary production. Glob. Chang. Biol. 9, 383–395. https://doi.org/10.1046/j.1365-2486.2003.00573.x.

Urbana-Champaign, B.G.| A.P., Dept of Agricultural and Consumer Economics, University of Illinois, 2025. Economic Outlook and Other Considerations for the 2025 Almond Pollination Season | West Coast Nut. URL. https://wcngg.com/2025/02/02/economic-outlook-and-other-considerations-for-the-2025-almond-pollination-season/ (accessed 4.3.25).

Vanella, D., Peddinti, S.R., Kisekka, I., 2022. Unravelling soil water dynamics in almond orchards characterized by soil-heterogeneity using electrical resistivity tomography. Agric Water Manag 269, 107652. https://doi.org/10.1016/j.agwat.2022.107652.

Vuppalapati, C., 2023. Specialty crops almonds. In: Vuppalapati, C. (Ed.), Specialty crops for climate change adaptation: strategies for enhanced food security by using machine learning and artificial intelligence, STEAM-H: Science, Technology, Engineering, Agriculture, Mathematics & Health. Springer Nature Switzerland, Cham, pp. 627–741. https://doi.org/10.1007/978-3-031-38399-1_7.

Wang, Z., Xiao, X., Yan, X., 2010. Modeling gross primary production of maize cropland and degraded grassland in northeastern China. Agric. For. Meteorol. 150, 1160–1167. https://doi.org/10.1016/j.agrformet.2010.04.015.

Webb, E.K., Pearman, G.I., Leuning, R., 1980. Correction of flux measurements for density effects due to heat and water vapour transfer. Q. J. R. Meteorol. Soc. 106, 85–100. https://doi.org/10.1002/qj.49710644707.

Wu, X., Zhou, J., Wang, H., Li, Y., Zhong, B., 2015. Evaluation of irrigation water use efficiency using remote sensing in the middle reach of the Heihe river, in the semi-arid northwestern China. Hydrol. Process. 29, 2243–2257. https://doi.org/10.1002/hyp.10365.

Xiao, X., Zhang, Q., Braswell, B., Urbanski, S., Boles, S., Wofsy, S., Moore, B., Ojima, D., 2004. Modeling gross primary production of temperate deciduous broadleaf forest using satellite images and climate data. Remote Sens. Environ. 91, 256–270. https://doi.org/10.1016/j.rse.2004.03.010.

Xiao, X., Zhang, Q., Saleska, S., Hutyra, L., De Camargo, P., Wofsy, S., Frolking, S., Boles, S., Keller, M., Moore, B., 2005. Satellite-based modeling of gross primary production in a seasonally moist tropical evergreen forest. Remote Sens. Environ. 94, 105–122. https://doi.org/10.1016/j.rse.2004.08.015.

Xue, J., Bali, K.M., Light, S., Hessels, T., Kisekka, I., 2020. Evaluation of remote sensing-based evapotranspiration models against surface renewal in almonds, tomatoes and maize. Agric Water Manag 238, 106228. https://doi.org/10.1016/j.agwat.2020.106228.

Yan, H., Fu, Y., Xiao, X., Huang, H.Q., He, H., Ediger, L., 2009. Modeling gross primary productivity for winter wheat–maize double cropping system using MODIS time series and CO2 eddy flux tower data. Agric. Ecosyst. Environ. 129, 391–400. https://doi.org/10.1016/j.agee.2008.10.017.

Zeri, M., Hussain, M.Z., Anderson-Teixeira, K.J., DeLucia, E., Bernacchi, C.J., 2013. Water use efficiency of perennial and annual bioenergy crops in Central Illinois. J. Geophys. Res. Biogeo. 118, 581–589. https://doi.org/10.1002/jgrg.20052.

Zhao, M., Running, S.W., 2010. Drought-induced reduction in global terrestrial net primary production from 2000 through 2009. Science 329, 940–943. https://doi.org/10.1126/science.1192666.